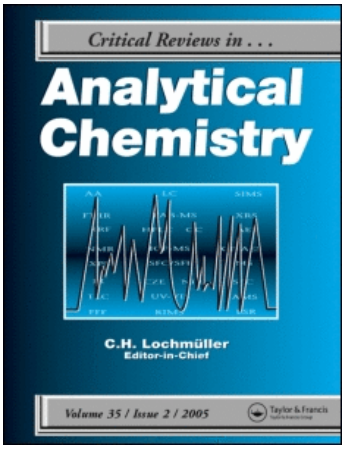

Critical Reviews in Analytical Chemistry
Publication details, including instructions for authors and subscription information:
http://www.informaworld.com/smpp/title~content=t713400837

A Review of Selected Highlights of Mössbauer Spectrometry

J. J. Spijkerman; P. A. Pella; J. J. Zuckerman

To cite this Article Spijkerman, J. J. , Pella, P. A. and Zuckerman, J. J.(1970) 'A Review of Selected Highlights of Mössbauer Spectrometry', Critical Reviews in Analytical Chemistry, 1: 1, 6 — 45
To link to this Article: DOI: 10.1080/10408347008542590
URL: http://dx.doi.org/10.1080/10408347008542590

A REVIEW OF SELECTED HIGHLIGHTS OF MÖSSBAUER SPECTROMETRY

Authors: J.J. Spijkerman and P.A. Pella
National Bureau of Standards
Washington, D.C.

Referee: J.J. Zuckerman
Department of Chemistry
State University of New York At Albany
Albany, New York

TABLE OF CONTENTS

INTRODUCTION

Mössbauer spectrometry is a nuclear resonance phenomenon which is exhibited in many nuclides with low-lying (less than 150 keV) excited states having lifetimes between 10^{-10} and 10^{-7} seconds. The Mössbauer spectral parameters of isomer shift, quadrupole splitting, and magnetic hyperfine splitting originate from the interaction of nuclear moments with extranuclear moments arising from the ground state electronic configuration and the surrounding lattice.

The isomer shift (displacement of the spectral line) arises from the Coulombic interaction between the nuclear charge and the effective electron density at the nucleus. Its magnitude is proportional to the difference in the nuclear charge radii of the ground and excited states and the total electron density at the nucleus. The isomer shift is primarily a measure of the s-electron density. But the presence of p-, d-, and f-electrons will indirectly influence the effective s-electron density at the nucleus, thereby affecting the isomer shift. Because the nuclear term is constant for a particular nuclide, the isomer shift is often indicative of the formal oxidation state and/or degree of covalent bonding.

The quadrupole splitting is derived from the electrostatic interaction of an aspherical nucleus with an asymmetric environment of electronic and lattice charges and is pertinent for structural information. The magnetic hyperfine splitting arises from the interaction of the nuclear magnetic moment with the effective magnetic field at the nucleus, producing the nuclear Zeeman effect. From studies of the internal magnetic field, information about electronic spin states, atomic spin distributions, and chemical bonding can be obtained. In many cases, the nuclear constants which enter into the respective expressions for the isomer shift, quadrupole splitting, and magnetic hyperfine splitting are not known. They can, however, be estimated by studying several Mössbauer levels of isotopes of one element.[1] Estimates could also be obtained from the study of members of an isoelectronic series such as Sn^{119}, Sb^{121}, Te^{125}, etc.,[2] and for the rare earths.[3]

A comprehensive compilation of review articles and references which describe the theory and practice of Mössbauer spectrometry in more detail is cited in the publications of DeVoe and Spijkerman[4,5] and in the data index of Muir, Ando and Coogan.[6] Some works[4,5,7] describe advances in such important areas as Mössbauer source preparation, detector considerations, cryostat technology, and others, and are a valuable source of information.

A survey of the ten-year history of Mössbauer spectrometry provides clear evidence of the interdisciplinary nature of this technique for the structural characterization of materials. Its versatility has been demonstrated in a variety of disciplines from nuclear physics to chemical catalysis. Although the phenomenon of nuclear resonance fluorescence has been shown for some 50 isotopes of about 20 elements, most of the applications have been concerned with Fe^{57}, Sn^{119}, Sb^{121}, I^{127}, and I^{129}. Of these, about 70% have focused on Fe^{57} and Sn^{119}. The widespread interest in these two isotopes arises from the fact that they have the most favorable nuclear characteristics. Furthermore, the availability of commercial Mössbauer sources and the relatively simple experimental methodology have contributed to their extensive use in Mössbauer studies.

An exhaustive review of only Fe^{57} and Sn^{119} applications still represents a formidable task. We have chosen, therefore, to select a limited number of publications, taken from various disciplines, in which the interpretation of the Mössbauer data provide a unique result and/or where information was obtained which could be compared to, or correlated with, other techniques such as X-ray diffraction, ESR, NMR, NQR, molecular spectroscopy, and magnetic susceptibility. To limit the scope of this review to basically physico-chemical applications, topics such as relativistic phenomena, nuclear parity, nuclear structure, and most of the experimental methodology were omitted.

INSTRUMENTATION

During the first decade since the discovery of the Mössbauer effect, spectrometer instrumentation has progressed from laboratory devices capable of demonstrating the phenomenon on γ-resonance fluorescence only to highly sophisticated research instruments. Precision spectrome-

ters and Mössbauer sources are now commercially available. With access to computers for data reduction, it is now feasible that Mössbauer spectrometry will become a standard technique in many more laboratories. Although spectrometers are now commercially available, it is instructive for the purposes of this review to describe some of the most salient features.

A Mössbauer spectrometer consists of two main parts, a velocity drive capable of producing the Doppler motion, and a gamma-ray detection system. Some of the earlier types of spectrometers used mechanical means for producing the Doppler motion, generally in the constant velocity mode. Although simple and reliable, they are, in general, difficult to interface to a multichannel analyzer, which is commonly used for automated data acquisition. The recent trend has been towards electromechanical velocity drive units coupled with multichannel analyzers operating in the constant acceleration mode. Such a system permits two methods for obtaining Mössbauer data conveniently. The first is the modulation of the pulse-height by the driving waveform, with the analyzer in the pulse-height analysis mode. A drawback with this system lies in the fact that the count-rate is restricted because of the long dead-time required to analyze and address each pulse into the memory. In addition, the analog-to-digital converter (ADC) must be linear. In the second method the analyzer is operated in a multiscalar mode using the address scalar to assign a constant increment of velocity to each channel. The main advantages of the latter method are that the dead-time is independent of channel number and that the ADC need not be linear. The accuracy of the data produced by this method, however, is only as good as the synchronization between the analyzer and the spectrometer.

For precise, step-wise scanning over limited regions of a Mössbauer spectrum, a constant velocity mode of operation is preferred. To obtain a constant velocity, the required input signal for the drive is a rectangular wave-function. The drive unit can generate this wave-function by means of a photocell which triggers a bistable circuit. The circuit could be designed so that the symmetry of the rectangular wave is variable thereby making it possible to generate velocities in the forward and backward direction. Non-symmetric spectra can, therefore, be studied with greater ease. Incorporation of the photocell system provides the benefit of generating rectangular waves without position drifts.

The electromechanical transducers used in Mössbauer spectrometers are notoriously non-linear. Therefore, they are most often used with an electronic feedback circuit to increase their linearity. The linearity of the transducer also depends to a great extent on the driving frequency. At frequencies below the mechanical resonance frequency, the required controlling force is a function of the spring constant of the transducer suspension and, hence, proportional to the displacement. Above the resonant frequency the required driving force depends upon the inertia (mass dependent) of the system. The motion of the transducer is nearly in phase with the applied force below the resonant frequency, whereas the motion is out of phase with the applied force above the resonant frequency. At the resonant frequency there is a 90° phase shift. For high performance, the driving frequency should be above the mechanical resonant frequency but should not be high enough to cause the system to be unstable. The optimum driving frequency will depend on the velocity range of interest and must, at the same time, be compatible with the production of the least amount of distortion. Normally, driving frequencies on the order of one to five Hertz are used.

The radiation detectors available include the proportional counter, the scintillation detector, and the solid-state detector. The proportional counter is generally employed in the energy region from one to twenty keV, and is extensively used for Fe^{57} spectroscopy. The filling gas usually consists of either argon, krypton, or xenon. Gas multiplication factors as high as 10^5 can be attained in these counters but at a considerable cost to the lifetime of the counter. With the advent of high gain solid state amplifiers, however, such large multiplication factors are no longer needed. Furthermore, the lifetime of the sealed proportional counter has been greatly extended through the use of CO_2 as the quenching gas. For Fe^{57} applications, a two-inch diameter counter filled with krypton at a pressure of one atmosphere is recommended. This counter is about 60% efficient and has a resolution of about 12%. For higher energies such as the

23.8 keV radiation of Sn^{119m}, the NaI (Tl) scintillation detector is preferable. A 2 mm NaI crystal is about 97% efficient for an energy of 23.8 keV, but the best energy resolution obtainable is about 20%. The solid-state detector has an extremely good energy resolution, 600 eV at 14.4 keV, but requires cooling to liquid-nitrogen temperature. In general, the cost and the relatively low counting efficiencies of the solid-state detectors in the energy range required have prevented their widespread use in Mössbauer spectrometry.

Because most Mössbauer sources are not monochromatic but emit a number of discrete γ- and X-ray energies, some means of discriminating between detector pulses which are proportional to these energies must be devised. This is usually done by a single-channel analyzer (SCA). The SCA selects only those pulses above a preselected threshold level, and within the "window" to be accepted and stored in the multichannel analyzer. This essentially ensures that only the Mössbauer γ-radiation is detected. Obviously any radiation which falls within the "window" of the SCA will also be detected and contribute to the background. The most convenient method of adjusting the SCA is by using the coincidence circuit of the multichannel analyzer in the pulse height mode.

There are a number of factors which contribute to distortions in a Mössbauer spectrum. Among these are moving-source geometry (inverse-square law) which produces a parabolic distortion of the baseline in the spectrum. This is particularly noticeable for a small source-detector distance. A moving-absorber-geometry will eliminate this distortion in the absence of Compton scattering. The parabolic distortion can also be decreased somewhat by reducing the transducer displacement. Another source of spectral distortion is manifested in so-called cosine smearing, which produces a spectral shift to higher velocities and is a direct consequence of the angular dependence of the Doppler effect. Finally, line broadening caused by a change in velocity can occur while counts are being accumulated in a multichannel analyzer. This is a function of the calibration constant (mm/sec/channel).

The velocity calibration of the spectrometer can be done by using a constant-velocity spectral measurement, or by using a known Mössbauer spectrum for comparison, as is usually the case for constant acceleration spectrometers. The National Bureau of Standards has issued a standard reference material for isomer-shift calibration[8] and will soon make available iron foil standards for velocity calibration. Optical techniques provide an absolute method for velocity calibration. By counting with a multichannel analyzer the fringes produced by a Michelson interferometer in conjunction with a laser light source, or by a moiré grating, the velocity for each channel can be measured. The interferometer can also be incorporated in the feedback loop of the transducer circuit for maximum accuracy and long-time stability.

Such factors as spectrometer vibration, nonlinearity of the drive, and zero-velocity drift will influence the accuracy and precision of the spectral parameters and should always be considered. The accuracy of the measured spectral parameters is normally derived from the computer analysis of the spectrum.[9,10] Protop et al.[11] have determined the standard error δv in the position expected for a single resonance line; this can be written:

$$\delta v = \frac{2\sqrt{2\Gamma_{exp}}}{\varepsilon_o\sqrt{\pi\eta}}\frac{1}{\sqrt{N}} \qquad (1)$$

where Γ_{exp} is the experimentally observed half-width, η is the calibration constant in millimeters per second per channel, ε_o is the fraction of Mössbauer absorption, and N is the total number of counts in the baseline. This expression permits the evaluation of the time necessary for the accumulation of the spectrum in order to achieve the desired precision in the line position.

APPLICATIONS OF MÖSSBAUER SPECTROMETRY

The isomer shift and quadrupole splitting are often considered together for the interpretation of chemical structure and type of bonding in compounds. For ease of presentation in this review, it is instructive to discuss the quadrupole splitting and isomer shift separately under the respective headings of chemical structure and chemical bonding. This somewhat arbitrary separation serves the purpose of demonstrating the

unique role that each of these parameters plays in chemical studies.

Chemical Structure

The quadrupole splitting, ΔE_q, arises from the interaction of the nuclear quadrupole moment with an aspherical charge distribution about the nucleus. Mathematically, the charge distribution is described by an electric field gradient tensor (EFG) whose principal components are V_{xx}, V_{yy}, and V_{zz}. For Fe^{57}, the quadrupole splitting is:

$$\Delta E_q = [(eQ)\ (eq)/2]\ [1 + \eta^2/3]^{1/2} \quad (2)$$

where eQ is the nuclear quadrupole moment, $eq = V_{zz} = \partial^2 V/\partial z^2$, and η is the asymmetry parameter given by $\eta = \frac{V_{xx} - V_{yy}}{V_{zz}}$ with the requirement that $|V_{zz}| \geq |V_{yy}| \geq |V_{xx}|$. The value of η ranges from 0 to 1. The quadrupole interaction produces a degenerate pair of nuclear spin states from the initial excited state of the Fe^{57} nucleus as shown in Figure 1 for $V_{zz} > 0$. The nuclear ground state with $I = 1/2$ remains unsplit. Therefore, the Mössbauer spectrum will consist of two lines whose separation is ΔE_q.

The EFG that the Fe^{57} nucleus experiences depends on the surrounding electronic configuration. Two most common coordination complexes of iron contain either four or six ligands around the metal ion in either a tetrahedral or octahedral configuration. In Figure 2 is presented the d orbital splitting pattern for ferric, d^5 and ferrous, d^6 iron in octahedral and tetrahedral fields. The "strength" of the ligand field will in each case determine whether the compound formed is high- or low-spin. Table 1 lists the values of the principal components of the EFG tensor for the five d orbitals. From this table it is possible to predict a quadrupole splitting in the Mössbauer spectrum at the limit of zero temperature for each of the electronic configurations in Figure 2. For example, octahedral and tetrahedral high-spin ferric complexes, each, have one electron in each orbital corresponding to a half-filled shell. The sum of each row in the table for one electron in each orbital is zero. Hence, no quadrupole splitting is expected from these valence electrons. A similar situation is found for octahedral and tetrahedral low-spin

FIGURE 1

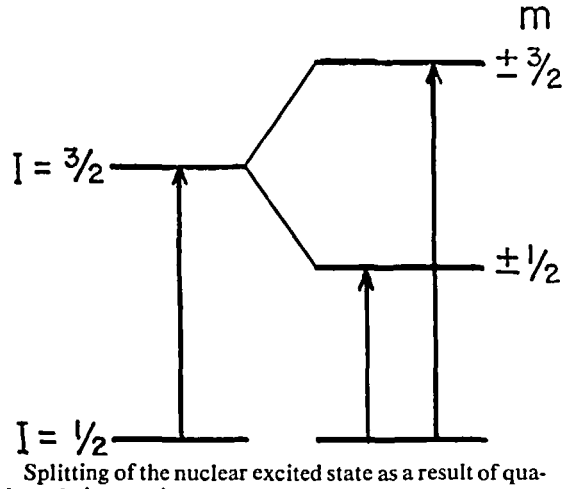

Splitting of the nuclear excited state as a result of quadrupole interaction.

TABLE 1

3d Orbital Contribution to the EFG Elements.*

Orbital	$V_{xx}/(qr^{-3})d$	$V_{yy}/(qr^{-3})d$	$V_{zz}/(qr^{-3})d$
d_{z^2}	−2/7	−2/7	+4/7
$d_{x^2-y^2}$	+2/7	+2/7	−4/7
d_{xy}	+2/7	+2/7	−4/7
d_{xz}	+2/7	−4/7	+2/7
d_{yz}	−4/7	+2/7	+2/7

*The charge q is equal to −e for an electron and +e for an "electron hole".

ferrous compounds. In the case of a nominally octahedral low-spin ferric complex at the zero temperature limit, one of the d_ϵ orbitals would contain only one electron where the other two orbitals would each be filled. Consequently, there is a vacancy or "hole" in one of the orbitals. Assuming the d_{xy} orbital contains the "hole" then the EFG values from the table are $+2/7e\langle r^{-3}\rangle$ for V_{xx}, $+2/7e\langle r^{-3}\rangle$ for V_{yy}, and $-4/7e\langle r^{-3}\rangle$ for V_{zz}. In a similar manner, the EFG values can be found for the d_{xz} and d_{yz} orbitals. Therefore, in the case of a vacancy in any of the three d_ϵ orbitals quadrupole splitting would be expected. By convention the principal component of the largest magnitude, i.e., $-4/7(V_{zz})$ for d_{xy}, $-4/7(V_{yy})$ for d_{xz}, and $-4/7(V_{xx})$ for d_{yz} orbitals, is chosen as the z axis of symmetry of the EFG tensor. Quadrupole splitting would also be expected for tetra-

FIGURE 2

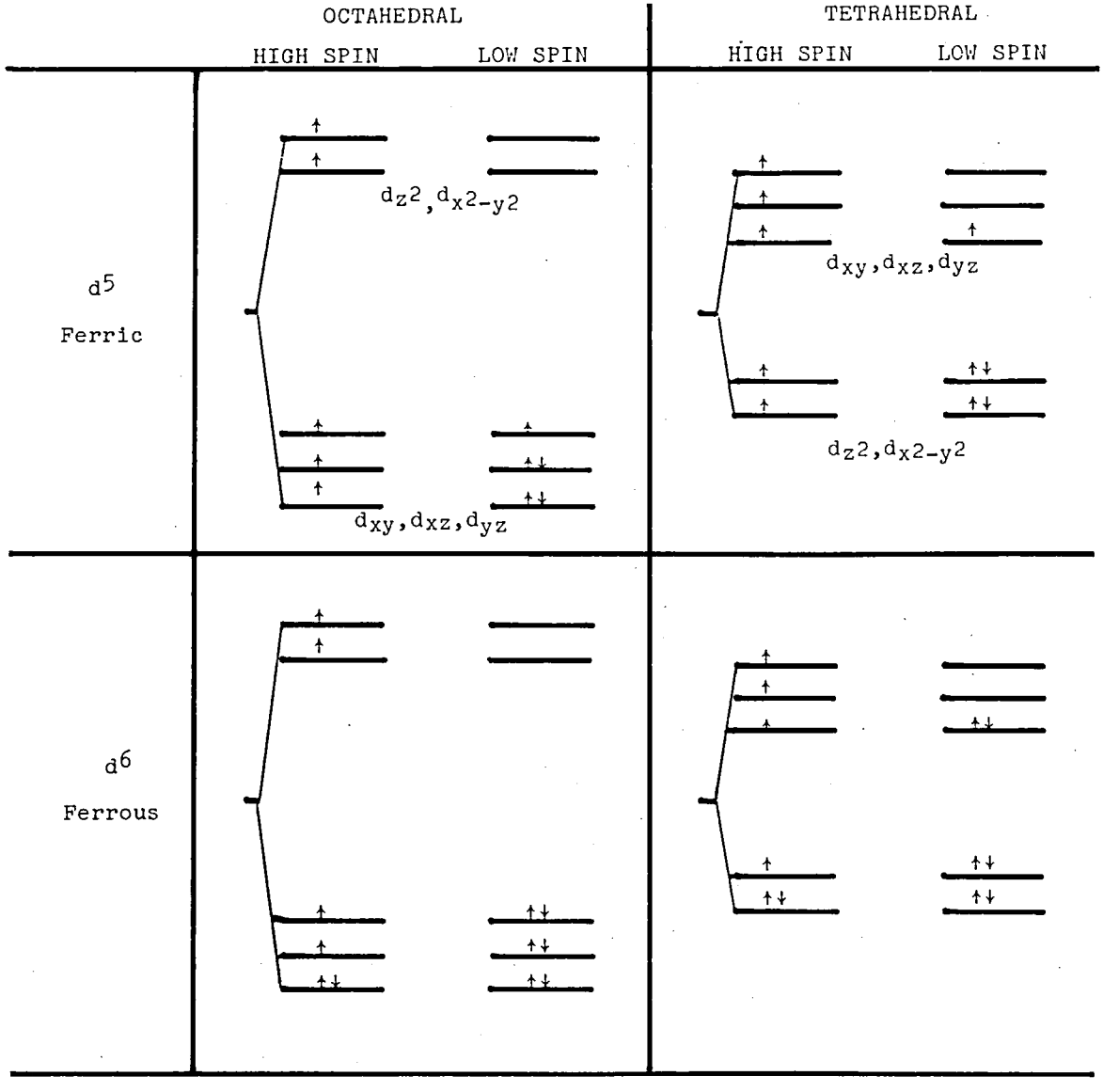

Electron population of d orbitals for various electronic configurations of iron in the presence of octahedral and tetrahedral ligand fields.

hedral low-spin ferric and octahedral high-spin ferrous, using similar arguments, because the extra electron outside the half-filled d shell is treated exactly like the "hole" case except that the charge q is negative.

Up to this point only the valence-electron contribution to the EFG has been considered. It is also possible to observe a ΔE_q arising from an aspherical charge distribution due to the neighboring ligands surrounding the metal ion. This is usually manifested by some distortion of the crystal lattice. For example, distortions from pure octahedral symmetry may arise as a consequence of dissimilar ligands; e.g., in MA_4B_2 complexes, or from a Jahn-Teller effect or a packing distortion produced by ions of different sizes.

Ingalls[12] has studied both the valence electron and the ligand contributions to the total EFG in high-spin ferrous compounds. His treatment is probably the most comprehensive to date. The principal component of the EFG tensor, eq, is rewritten by Ingalls as:

$$q = \frac{V_{zz}}{e} = (1 - R)q_v + (1 - \gamma_\infty)q_{lat} \quad (3)$$

where q_v and q_{lat} refer to the EFG values produced by the valence electron and ligand charge distributions, respectively, and R and γ_∞ are the appropriate Sternheimer anti-shielding factors. The crystal symmetry considered was that of an octahedron with tetragonal (axial symmetry) and rhombic distortions. Most transition metal complexes show the effects of distortion produced by asymmetric ligand fields on the metal ion ground term, excited term, or both. The energy level scheme is shown in Figure 3. The axial distortion is represented in the figure as a compression of the axial ligand-metal ion bond. This causes the orbitals containing z character to lie higher than those containing xy character. An elongation along the z axis would produce the opposite effect, reversing the order of the d_{z^2} and $d_{x^2-y^2}$ orbitals, and reversing the d_{xy} with respect to the d_{xz} and d_{yz} orbitals. The effect of the rhombic field can be represented by a change of the metal-ligand distance in the x-y plane of the octahedron. This is illustrated in the energy level scheme by the splitting of the degenerate d_{xz}, d_{yz} orbitals with the d_{xz} orbital lying highest. An expression for the quadrupole splitting was derived by which the crystal-field distortion parameters Δ_1 and Δ_2 could be calculated in terms of a reduction factor, F, and is:

$$\Delta E_q = (2/7)e^2Q(1 - R_o)\langle r^{-3}\rangle_o \alpha^2 F(\Delta_1, \Delta_2, \alpha^2, \lambda_o, T) \quad (4)$$

where α^2 is a covalency factor and λ_o is the spin-orbit coupling parameter. By means of computer techniques, initial estimates Δ_1 and Δ_2 are made and F is plotted versus Δ_1/λ and Δ_2/λ for each temperature, assuming the free-ion value for λ. Iterative refinement of F gives a value of ΔE_q which can then be compared with experimental values. Ingalls mentions that a possible weakness in his treatment is that the calculated distortion parameters are not unique, since the values were chosen to fit only the Mössbauer data over a wide temperature range. However, the estimates of the parameters so obtained are generally consistent with those from other methods. Webb[13] has compared the values of Δ obtained from Mössbauer data with those obtained by other methods for various compounds. He concludes that the absolute values themselves should not be interpreted too literally but, more important, are the general trends observed in most cases. In principle, the magnitude and sign of Δ could be obtained by: (a) single-crystal magnetic susceptibility and ESR measurements at one temperature; (b) variable-temperature susceptibility and Mössbauer measurements on a polycrystalline sample; and (c) single-temperature ESR measurements on powders and proton NMR spectra of solids and solutions at known temperatures.

In Ingalls' treatment, q_v was considered to be larger than q_{lat} in terms of their respective contributions to the total EFG. Nozik and Kaplan[14] have considered the lattice contribution in several ferrous compounds. For $FeSiF_6 \cdot 6H_2O$, q_{lat} was found to be quite small, but it was relatively large for $FeCl_2 \cdot 4H_2O$. Some of their results did not agree with those obtained by Ingalls and the cause of this discrepancy is not fully understood. Furthermore, these authors pointed out that the assumption that the lattice

FIGURE 3

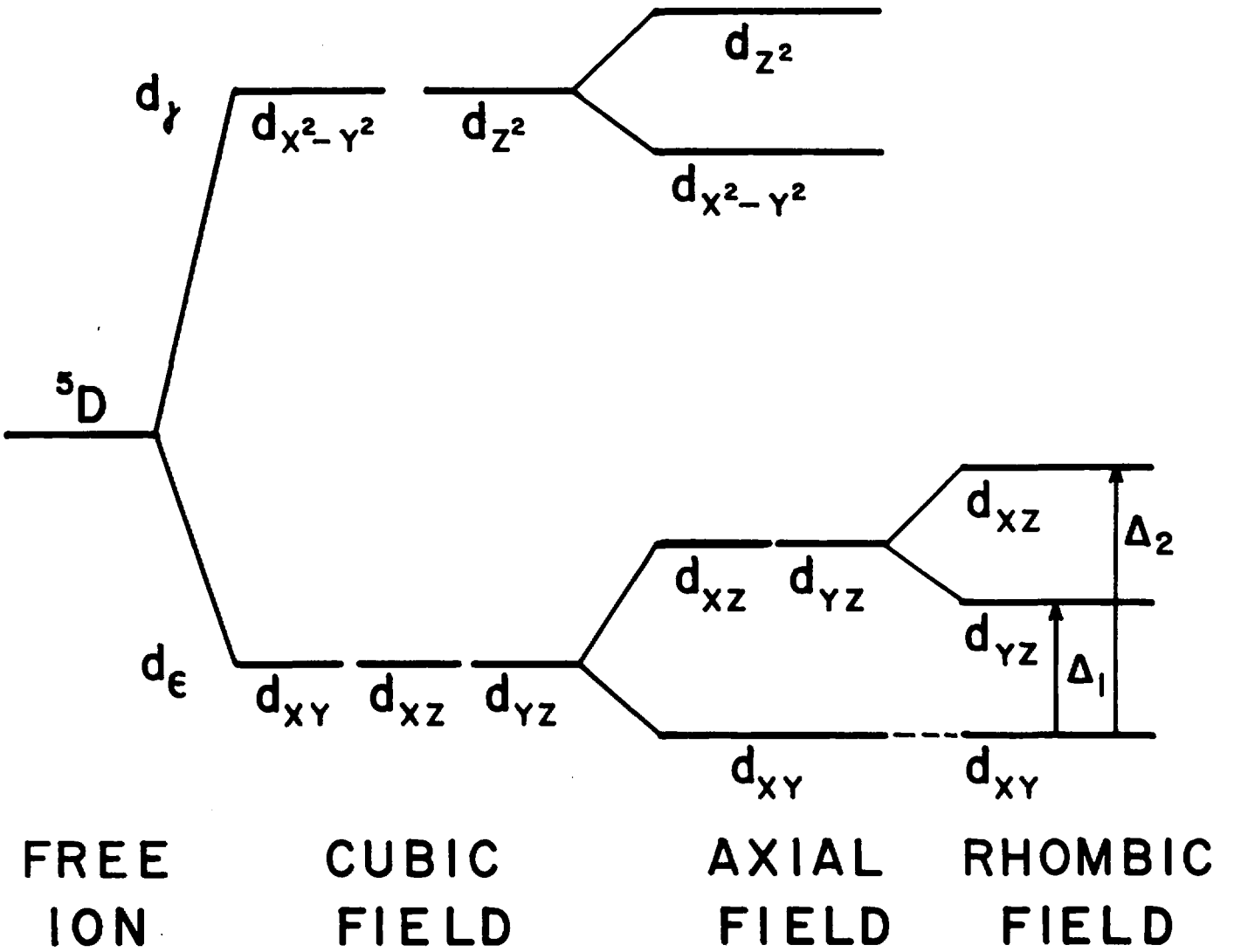

Energy level scheme for the ferrous ion in the presence of axial and rhombic fields.

contribution is small and can be neglected is not correct. The resolution of this question is important because such factors as the magnitude and sign of the lattice contribution to the EFG will affect the calculated value of the quadrupole moment and will influence the validity of conclusions regarding ligand symmetry, orbital splittings, and spin-orbit interactions in ferrous compounds.

Clark et al.[15] investigated the mineral gillespite, $BaFeSi_4O_{10}$, which contains high spin Fe(II) in square-planar coordination. The quadrupole splitting was correlated with magnetic susceptibility and electronic spectra. The lattice and valence contributions were found to have opposite signs with the lattice contribution slightly larger in magnitude. The authors stated that this result was most unusual in high-spin ferrous compounds. It was emphasized that the valence contribution was almost completely independent of temperature in the range studied.

A determination of the sign of V_{zz} can provide additional information about chemical structure. In complexes where axial distortion is present and $V_{xx} = V_{yy}$ (i.e., $\eta = 0$), the sign of V_{zz} can give the ground state orbital directly. An elongation or compression of the axial metal-ligand bond can be determined this way. Because the experimental spectrum shows just two quadrupole split lines for Fe^{57}, the problem is one of deciding which line corresponds to the $|\frac{1}{2},\pm\frac{1}{2}> \rightarrow |\frac{3}{2},\pm\frac{1}{2}>$ nuclear transition and which to the $|\frac{1}{2},\pm\frac{1}{2}> \rightarrow |\frac{3}{2},\pm\frac{3}{2}>$ transition. The sign of V_{zz} is shown for either case in Figure 4. If an external magnetic field of about 30 kOe is applied perpendicular to the direction of the γ-rays, one of the lines will split into a doublet and the other into a triplet. The doublet corresponds to the $\pm 3/2 \rightarrow \pm 1/2$ transition and the triplet to the $\pm 1/2 \rightarrow \pm 1/2$ transition. A doublet at positive velocities means that the $\pm 3/2$ is highest and $V_{zz} > 0$. Conversely, when $V_{zz} < 0$ the doublet occurs at negative velocities.

Dale et al.[16] have used this approach to determine the nature of the distortion in low-spin Fe(II) compounds. There was no valence electron contribution to the EFG in these compounds because they were diamagnetic. Large quadrupole splittings were observed for $PcFe(Py)_2$, $Fe(niox)_2(Im)_2$, and $Fe(niox)_2(NH_3)_2$ at 4.2°K.* It was suggested that the EFG in these compounds was generated mainly by anisotropic covalent bonding (notably the σ bonding). The sign of the EFG was positive (i.e., $V_{zz} > 0$); this implies an elongation along the axial z axis. For $Fe(niox)_2(Im)_2$ the spectrum was not clearly resolved into a doublet and triplet, and this suggests that the condition $V_{xx} = V_{yy}$ is not met. The sign of the EFG in such cases is ambiguous. In order to explain the large asymmetries observed, Dale proposed that the difference in the ligand field produced by a $-N=O$ group as opposed to a $-N-OH$ group may be responsible. In addition, the possibility that the nioxime ligands carry residual negative charges residing largely on the oxygen atoms should also be considered.

Determination of the sign of the EFG for ferrocene by Collins[17] has led to a choice between the crystal field treatment[18] which predicted a positive EFG, and the molecular orbital (MO) treatment of Ballhausen et al.[19,20] which predicted a negative EFG. With an applied magnetic field of 40 kG, the two lines split clearly into a doublet and a triplet. The Mössbauer results were consistent with the MO treatment.

Edwards and Johnson[21] reported on a series of tetrahedrally coordinated compounds of the type R_2FeX_4, where X is a halide or pseudohalide and R is a quaternary ammonium or phosphonium cation. From magnetic susceptibility measurements iron was identified as high-spin Fe(II). The degree of distortion from "cubic" symmetry was dependent on the ligand X and cation R. For large R, the quadrupole splitting was studied as a function of temperature and interpreted as a static distortion which splits the d_{z^2} and $d_{x^2-y^2}$ by an energy $\Delta = 470 cm^{-1}$. For $(NMe_4)_2FeCl_4$, the Mössbauer data could not be fitted with the derived expression over the whole temperature range especially at the high temperature end. To explain the de-

*Pc = phthalocyanine
niox = 1,2-cyclohexanedioxime mono-anion
Im = imidazole
Py = pyridine

FIGURE 4

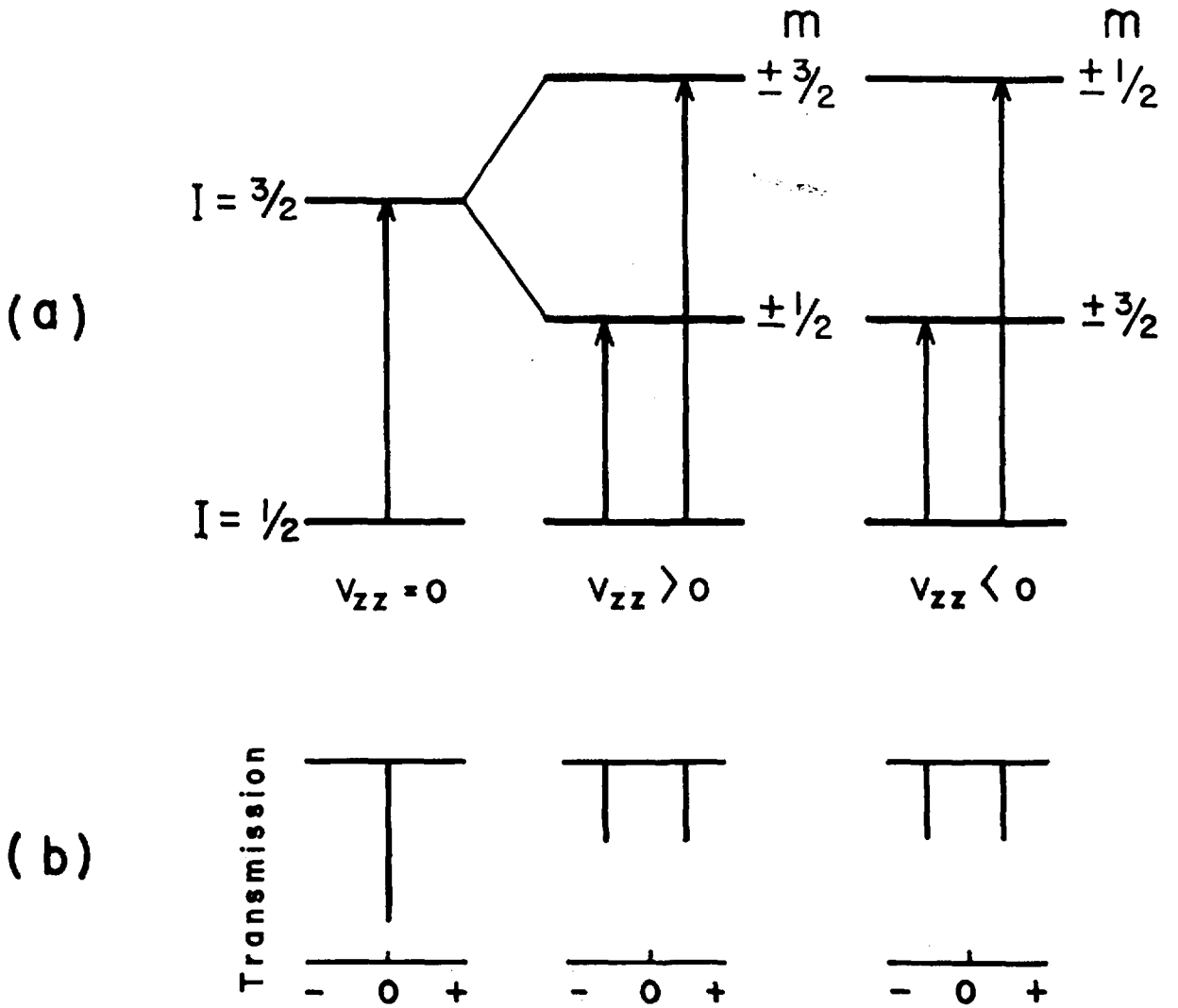

(a) Nuclear energy levels for Fe^{57}; (b) Mössbauer line spectra for Fe^{57}

crease in ΔE_q for this compound two plausible mechanisms were proposed. First, an expansion of the 3d orbitals onto the ligands decreases the value of $\langle r^{-3}\rangle_{3d}$. Secondly, some 4p character may be mixed into the metal-ligand bonds. This results in a smaller effective value for the EFG. A 4p-electron contributes $+4/5\langle r^{-3}\rangle_{4p}$, whereas a 3d-electron contributes $+4/7\langle r^{-3}\rangle_{3d}$ where $\langle r^{-3}\rangle_{4p}$ is less than $\langle r^{-3}\rangle_{3d}$. Such arguments are only qualitative at best and demonstrate the need for further study of all the factors which influence ΔE_q. However, the sign of the EFG for $(NMe_4)_2FeCl_4$ at 81°K was negative which indicated that the ground state orbital was d_{z^2} undergoing a compression along the z axis. Some interesting conclusions were also drawn regarding the isomer shift. Comparison of tetrahedral Fe(II) compounds with the analogous octahedral high-spin Fe(II) compounds with similar ligands coordinated to the metal ion indicates that the coordination number could be determined by the isomer shift values.

The sign of the EFG can also be determined by measurements on single crystals. The Mössbauer absorption spectrum is studied as a function of crystal orientation or through the use of a polarized γ-ray source. From ESR measurements Spijkerman et al.[22] have shown that the sign of the zero field splitting parameter, D, may be found from Mössbauer studies at about 1°K where $kT<|2D|$.[13] This is an additional way of obtaining the sign of ΔE_q from the relationship

$$D = D_o + \frac{k}{nKq}\Delta E_q \qquad (5)$$

Chemical Bonding

The isomer shift can often give a direct or indirect measure of the role of s-electrons in chemical bonding. This hyperfine interaction measures primarily the differential s-electron density at the nucleus between the source and the absorber. An expression can be written:

$$\text{I.S.} = F(Z)\Delta R/R[|\Psi_s(o)|^2 - |\Psi_A(o)|^2] \qquad (6)$$

where F(Z) represents a composite of nuclear terms, $\Delta R/R$ is the relative change in the average radius of the nuclear charge distribution from the ground to the excited state, and $|\Psi_s(o)|^2$ and $|\Psi_A(o)|^2$ are the s-electron densities at the nucleus for the source and absorber, respectively.

Isomer Shift for Fe^{57}

Walker et al.[23] presented a correlation diagram for di- and trivalent inorganic compounds of iron. Using Watson's Hartree-Fock calculations for various configurations of iron (such as $3d^y4s^x$), the total s-electron density for different numbers of d-electrons was plotted versus the percentage 4s-electron contribution. The observed isomer shifts were then calibrated in terms of the total s-electron density. It was assumed that the observed isomer shifts for the most ionic divalent and trivalent compounds corresponded to those for pure $3d^6$ and $3d^5$ electronic configurations, respectively. A prediction of 4s orbital occupation could be made from this diagram from the observed isomer shifts of iron compounds. Though this correlation has met with moderate success, some discrepancies have been found. Recently, more elegant approaches for predicting 4s-orbital occupations have been employed using molecular orbital calculations.[24] Deviations from the treatment of Walker et al. are apparent, particularly where covalency effects are present, that is, where an appreciable interaction exists between d-electrons of the metal with ligand orbitals. For high-spin iron compounds, the s-electron density at the nucleus depends strongly upon the shielding effect of the 3d-electrons. As the population of the 3d orbitals increases, so does the effect of shielding on the s-electrons. Because the sign of $\Delta R/R$ for iron is negative, a decrease in s-electron density gives rise to a positive isomer shift. In low-spin compounds the situation is different. In such compounds the 3d-electrons of the metal are delocalized with ligand orbitals of appropriate symmetry. This covalent bonding results in a reduced shielding efficiency of the 3d-electrons. Consequently, the observed isomer shift is much smaller than for the high-spin compounds. Danon[25] has classified the isomer shift for low- and high-spin compounds in the order:

$$Fe^{+2}(\text{ionic}) > Fe^{+3}(\text{ionic}) > Fe^{+2}(\text{cov}) > Fe^{+3}(\text{cov})$$

For the complexes $Fe(III)(CN)_6^{-3}$, $Fe(CO)_5$, and $Fe(II)(CN)_5(NO)^{-2}$ containing isoelectronic ligands, the order of s-electron density was given: $CN^- < CO < NO^+$. This trend also follows the order of increasing ligand electronegativity. To describe the bonding in $Fe(II)(CN)_5$

$(NO)^{-2}$, Danon[26] invokes the concept of "back donation" where the d_{Π} electrons of the metal are transferred to the Π^* (antibonding orbital) of the nitrosyl ligand. This mechanism would give rise to an increase of s-electron density by decreasing d-electron shielding. Comparison of the Fe-NO distance (1.63A°) with the Fe-CN distance (1.92A°) seems to support this interpretation. Shulman and Sugano[27] have used a molecular orbital treatment of the iron complex cyanides and point out the role of empty antibonding ligand orbitals in the covalent bonding in such complexes. On the basis of these MO calculations, the similar isomer shifts observed for the ferro- and ferricyanides were explained.

Isomer shifts were reported for a number of Fe(II) complexes of phenanthroline and its derivatives substituted in the 5-position.[28] In the homologous series the atoms bonded to the iron were the same; i.e., N, and the spatial distributions about the iron atom were the same. Changing the ring substituents did not affect the isomer shift values throughout the series enough to be conclusive. For many organo-iron and organotin complexes, substitution of aromatic moieties does not measurably affect the s-electron density at the nucleus. Hence, the isomer shift in many cases is not sensitive to such changes.

Large isomer shifts were observed in compounds of the type $L \rightarrow Fe(CO)_4$ studied by Collins and Pettit.[29] The variation in isomer shift was explained by the Lewis base (electron-donating) strength of the ligands. The formation of a σ-bond between ligand and metal resulting in "forward-coordination" produced a sizable change in the s-electron density. The mechanism of back donation could also lead to essentially the same interpretation. A large change in isomer shift was observed when the sulfur ligand was replaced by phosphorus in the cyclopentadienyl (Cp) derivatives $Cp(OC)Fe(SMe_2)_2$ $Fe(CO)Cp$.[30] It was concluded that sulfur is a less effective σ-electron donor than phosphorus in these compounds.

It is perhaps instructive at this point to make some generalizations about the isomer shift in iron compounds. For iron in the high-spin configuration, the isomer shift is usually indicative of the formal oxidation state. In the low-spin configuration, the isomer shift is not sensitive to oxidation state. The variation of isomer shift in high-spin complexes is due to varying degrees of 4s orbital occupation. In low-spin complexes differences in s-electron density as a result of delocalization of 3d-electrons with II orbitals of the ligand should be considered. It should also be noted that even if 4s orbital occupation increases, the delocalization of d and p orbitals may offset this increase at the iron nucleus. Much useful information could be obtained from the study of the isomer shift in an homologous series, especially about relative chemical bonding. But it seems that Mössbauer data in combination with other spectroscopic techniques and molecular orbital calculations would result in a much clearer overall picture.

Isomer Shift in Sn^{119}

A number of systematic studies of the isomer shift have been reported for tin compounds. Cordey-Hayes[31] has classified 20 or more inorganic tin compounds into two distinct groups. With respect to white tin metal, positive isomer shifts correspond to Sn(II), while negative isomer shifts correspond to Sn(IV) compounds. The compound Cs_2SnF_6 came closest to being completely ionic Sn(IV) (i.e., $4d^{10}$ configuration), while $SnCl_2$ was nearest the covalent $4d^{10}5s^2$ configuration. The isomer shifts for Sn(IV) halides were correlated with the electronegativity difference of the halide ions and a linear relationship was found.[32] No similar relationship existed for Sn(II) halides.

Zuckerman[33] has critically examined the proposed correlation of isomer shift with percentage ionic character with reference to a homologous series of stannous and stannic compounds. His conclusion was that the tin isomer shift could not be correlated in any meaningful way with the ionic character of the chemical bonds.

Lees et al.[34] have given an interpretation of the isomer shift in Sn(II) compounds. A linear relationship between the isomer shift and the quadrupole splitting was found for a number of Sn(II) compounds. Two straight lines having different slopes (by about a factor of 2) were drawn through a series of points representing two distinct families of tin(II) compounds as shown in Figure 5. The intercept which corresponds to zero ΔE_q yielded the isomer shift for the ionic $5s^2$ configuration. Their interpretation suggested that covalent bonding is present in ad-

FIGURE 5

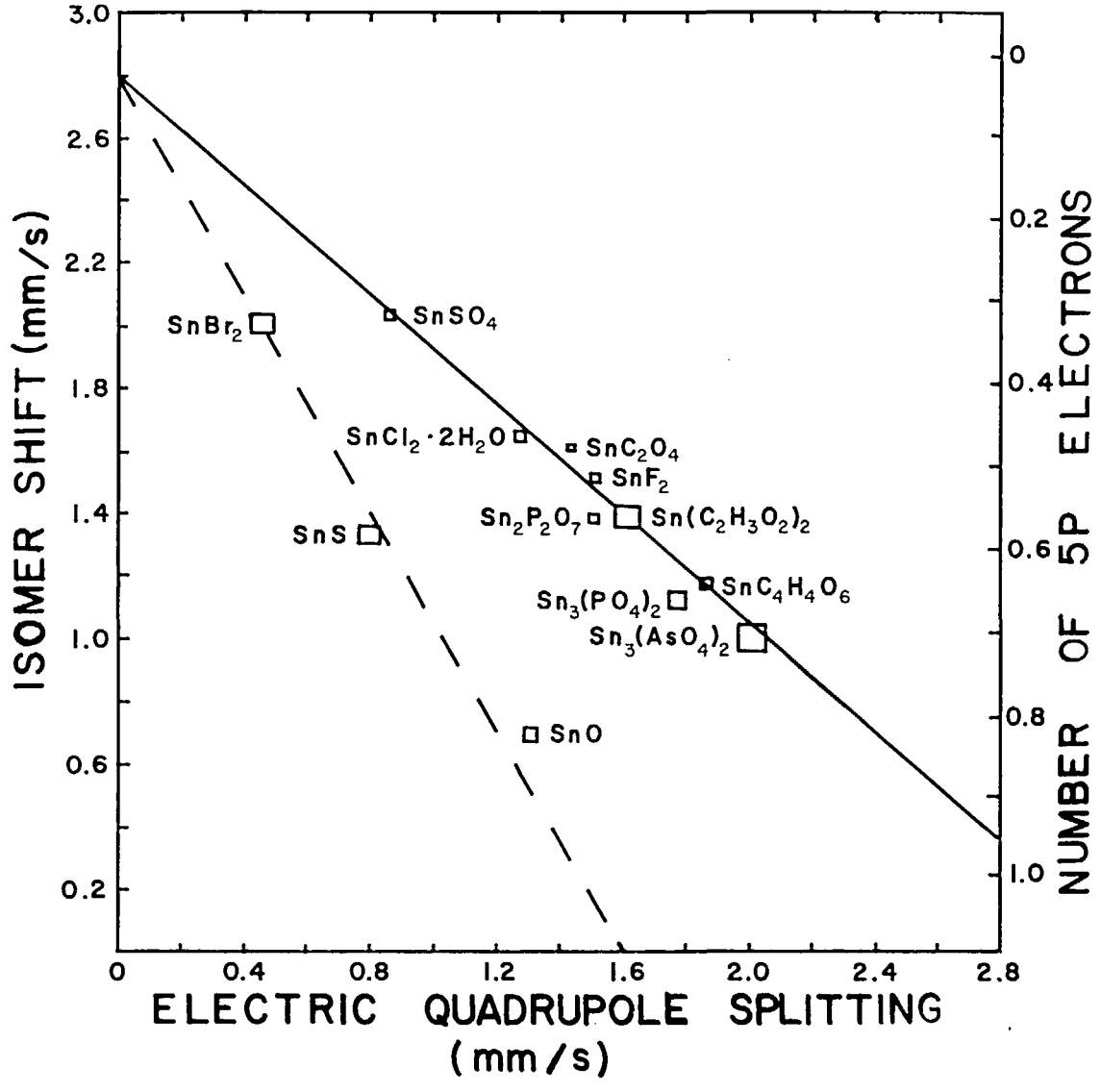

Isomer shifts versus quadrupole splittings for various Sn (II) compounds. Lees, J. and Flinn, P.A., *Phys. Lett.*, 19, No. 3, 187, Oct. 1965. With permission of North-Holland Pub. Co., Amsterdam.

dition to some ionic bonding in Sn(II) and that the configuration $5s^2$ contains some 5p character admixed. An increase in p-like character with a corresponding decrease in s-like character, both, contribute to a change in isomer shift. The differences in the two families of compounds were attributed to differences in covalent bonding. The compounds on the upper line were those in which the covalent bond was linear with only p_z orbital contribution from the stannous ion. The bonding in those on the lower line was predominantly planar, involving equal amounts of p_x and p_y contributions.

Zuckerman et al.[35,36] have tested this two-line plot. A series of tin(II) compounds was synthesized in which the tin atom was held in a small ring. The isomer shift and quadrupole splitting data for these organometallic compounds were found to lie on the upper branch of Figure 5. This would indicate that the O-Sn-O bond was linear. It was noted, however, that the bond could not possibly be linear because of the stereochemistry of the five- and seven-membered rings. Kamenar and Grdenic[37] have shown that $SnCl_2 \cdot 2H_2O$ which falls on the upper line has a structure in which the tin atom is pyramidal. It appears that no really satisfactory relationship has been found between the isomer shift and the quadrupole splitting for either valence state of tin.

Covalent sp^3 hybridization has been considered in the isomer shift interpretation of Sn(II) compounds by Donaldson et al.[38] The order of the isomer shifts was correctly predicted for SnTe, SnSe, SnS, SnI_2 and $SnCl_2$. Positive shifts for SnO and SnF_2 were observed which did not fit the data. No satisfactory explanation of the anomalous isomer shifts for these two compounds has as yet been suggested. It was observed that in any series of Sn(II) compounds, the change in isomer shift was always inversely proportional to the amount of sp^3 character in the bond. Correlations of isomer shift with the polarizing power of M in $MSnF_3$ and MSn_2F_5, where M = Cs, Rb, K, Na, Ba, or Sn, were also reported by these authors. The increase in isomer shift was attributed to the polarizing power of M. As the polarizing power increases, the weaker the Sn-F bond becomes which gives rise to a larger positive isomer shift.

A compound which exhibits an appreciable quadrupole splitting is SnF_4. In the solid the tin atom is at the center of a distorted octahedron with four fluorine atoms forming linear bridging between neighboring tin atoms (the Sn-F distance is 2.04 Å) while the other two fluorine atoms are directly bound to only one tin atom (Sn-F distance is 1.879 Å).[39] The large value of ΔE_q was attributed presumably to the inequivalence of fluorine atoms in the crystal structure. This could be represented by $F^{\delta-}(SnF_2)^{2\delta+}F^{\delta-}$.

The interpretation of the isomer shift for tin has been complicated by disagreement over the sign of $\Delta R/R$. It was not until the definitive experiments of Bocquet et al.[40] at Brookhaven that this question became finally resolved. With Sn^{119m} sources of white tin metal and SnO_2, high-resolution internal conversion measurements were made of the electron lines from the 23.87 keV M1 transition. The 5s (valence-shell) electron density found at the nucleus was 30% smaller in SnO_2 than in white tin. From the electron densities and the observed isomer shifts, $\Delta R/R$ was calculated and found to be $+3.3 \times 10^{-4}$ with an uncertainty of about 30%. This result confirmed the original conclusions of Lees and Flinn, Kistner, Jaccarino and Walker, and others,[41-44] but disagreed with those of Bersuker, Goldanskii and Makarov.[45]

A study of hexacoordinated Sn(IV) compounds revealed an absence of quadrupole splitting even when the tin atom was in an environment which deviated considerably from octahedral symmetry.[46] The compounds were of the type SnX_6^{-2} where X = Cl, Br, or I, and SnX_4L where L was a bidentate ligand. A rule based on the measurement of more than 24 compounds was proposed. For hexacoordinated Sn(IV) compounds, zero quadrupole splitting would be expected provided that all the various atoms surrounding the central tin atom had non-bonding p_π electrons. This rule was applied to elucidate the nature of the 1:1 compound formed between Sn(IV) chlorides and N_2O_4. Infrared data[47] indicated that the structure was probably $NO^+[SnCl_4NO_3]^-$ and suggested that the nitrate ion was bidentate. A unidentate nitrate ion would result in a pentacoordinate tin complex with a large quadrupole splitting. A bidentate one would yield a single line for a hexacoordinated complex as was observed from Mössbauer

spectra.

A correlation of decreasing isomer shift with increasing electronegativity of the halide ions was noted for the series SnX_4-bipy and $SnX_2\{[Ph_2P(O)]_2N\}_2$.[46] Evidence of the influence of electron delocalization effects was found in these tin chelate systems. The π-interactions influence the shielding efficiencies of orbitals surrounding the tin nucleus and thus affect the s-electron density and isomer shift. Comparison of $SnCl_4$·bipy*($\delta = 0.42$), $SnCl_4$·oxH*($\delta = 0.42$), and $SnCl_4[Ph_2(O)_2]NH$($\delta = 0.40$mm/sec) showed that the isomer shift values were approximately the same whether two chlorine atoms in $SnCl_6^{-2}$ are replaced by two nitrogen atoms, a nitrogen and an oxygen atom, or two oxygen atoms. However, when two additional chlorine atoms are replaced to give the series $SnCl_2L_2$, there was a variation in isomer shift over the range of 0.25mm/sec. The inductive effect of the methyl group in Me_2SnCl_2·bipy ($\delta = 1.55$mm/sec) was suggested as the cause of the change in isomer shift from that in $SnCl_4$·bipy ($\delta = 0.42$mm/sec).

Interpretation of the isomer shift for tin compounds should take into account important screening effects produced by: (a) shielding of 5s by 5p electrons, (b) mutual shielding of paired 5s electrons characteristic of the divalent state, and (c) changes in the shielding of the inner electrons by outer valence electrons.[31]

Magnetism

One of the most exciting areas of Mössbauer applications is in the study of the magnetic properties of materials. This includes such phenomena as ferromagnetism (where the electron spins are aligned in the same direction), antiferromagnetism (where the spins are equal in magnitude but aligned in opposite directions), ferrimagnetism, and paramagnetism.

Magnetic hyperfine splitting (nuclear Zeeman effect) arises because of the interaction between the nuclear magnetic moment and the magnetic field produced by the extranuclear electrons. This interaction produces an effective magnetic field at the nucleus which can be observed by the Mössbauer method. For a nucleus with $I>0$, the magnetic interaction splits the nuclear levels into $2I + 1$ components. For Fe^{57} a six-line Zeeman pattern is observed.

The effective magnetic field at the nucleus, H_n, consists of a sum of several contributions of which the most predominant are: H_s, H_L and H_D. H_s is the spin density field or as it is often called, the core polarization field. It is produced by an electron-spin exchange interaction between polarized 3d electrons and the inner core 1s, 2s, and 3s electrons. Depending upon the relative electron-spin orientation in the respective shells, an exchange interaction can produce a magnetic asymmetry between the inner core s-electrons. This gives rise to a net spin density at the nucleus. Another commonly used term to describe this particular mechanism is the Fermi contact interaction. It is also the primary contribution to the effective magnetic field for ferro-, ferrimagnetic, and paramagnetic materials. H_L is the field produced by the orbital angular momentum of the electron, and H_D is the field produced by spin-orbit coupling.

The application of an external magnetic field can be used to study the atomic spin distribution in magnetic materials. For example, atomic spins of ferromagnetic materials will tend to align themselves parallel to the external magnetic field. By inspection of the absorption line intensities or by noting whether certain lines are absent, the atomic distribution can be found.

The magnetic properties of hematite, or α-Fe_2O_3, have been extensively studied.[48-52] Great interest in this compound was inspired by the fact that it exhibits a magnetic "spin-flop" phenomenon above or below a characteristic temperature called the Morin temperature, T_M. α-Fe_2O_3 has an important place in the historical development of Mössbauer spectrometry because it was in this compound that Kistner and Sunyar[53] first observed a quadrupole interaction and isomer shift.

Below T_M(260°K) α-Fe_2O_3 is antiferromagnetic and the magnetic moments lie parallel to the [111] crystallographic plane. Above 260°K the moments of the paired atoms lie in the basal [111] plane and are not precisely antiparallel, but are canted slightly towards one another in the basal plane. This gives rise to a weak ferromagnetism. The transition from the

*bipy = bipyridyl
oxH = 8-hydroxyquinoline

antiferromagnetic to the weakly ferromagnetic state or vice versa is known as the "spin-flop" phenomenon. This can be brought about by the application of an external magnetic field (60-70 kOe) along the [111] direction below the Morin temperature. Consequently, the antiferromagnetic α-Fe_2O_3 can be induced to "flop" into the high temperature configuration. This will occur at some critical value of the applied magnetic field.

The observation of "spin-flop" by Mössbauer spectrometry is based on the angular dependence of the relative spectral line intensities of a single crystal of α-Fe_2O_3. The two lines in the Mössbauer spectral pattern corresponding to $\Delta m = o$ transitions have an angular dependence of $\sin^2\Theta$, where Θ is the angle between the spin orientation axis and the γ-ray direction. If the crystal is oriented so that the γ-rays propagate along the [111] axis, then the two lines corresponding to $\Delta m = 0$ will be absent below T_M and will reappear on warming through T_M. This is a rather dramatic demonstration of the "spin-flop" phenomenon. Figure 6 illustrates the changes in the Mössbauer spectrum in going through the Morin temperature.

Simkin et al.[52] have observed a monotonic decrease in the Morin temperature from 263 to 246°K when magnetic fields from 0 to 9 kOe were applied. The results were found to be consistent with the thermodynamic treatment[54,55] describing the magnetic behavior of α-Fe_2O_3.

Two internal magnetic fields at the iron nuclei were found in goethite (α-FeOOH) by Hrynkiewicz et al.[56,57] at room temperature. Both magnetic field intensities fell with increasing temperature. H_1 disappeared at about 340°K and the other, H_2, at about 370°K. Such behavior was explained by assuming the existence of four magnetic sublattices in α-FeOOH and was in agreement with a theoretical prediction.[58] Two of the sublattices were responsible for the field at H_1 and the other two for H_2. If the position of the hydrogen ions were asymmetrical with respect to the two oxygen ions, this could account for the different magnetic sublattices.

In the study of magnetite, Fe_3O_4, Verwey proposed a hypothesis to explain the marked changes in physical properties exhibited between 110° and 120°K. A sharp decrease in electrical conductivity as well as changes in magnetization and specific heat behavior were observed. He suggested that there is a transition of the order-disorder type which may account for the electrical conductivity behavior. Magnetite has an inverse spinel structure and can be represented by the formula $Fe^{3+}[Fe^{2+}Fe^{3+}]O_4$.[59-62] The unit cell consists of eight ferric and eight ferrous ions as octahedral sites (B sites), each with six oxygen nearest neighbors, and eight ferric ions at tetrahedral sites (A sites), each with four oxygen nearest neighbors. Verwey proposed that above the transition region there is a dynamic disorder caused by a fast electron exchange between the ferric and ferrous ions in the octahedral sites, which leads to an increase in electrical conductivity. Below the transition region, the ferric and ferrous ions in the octahedral sites are ordered separately. The ordered arrangement had possessed orthorhombic, whereas the disordered lattice possessed cubic symmetry.

In 1961 Bauminger et al.[63] measured the internal magnetic field acting on the iron nuclei in magnetite. Two distinct effective magnetic fields were measured. At 300°K, H_{eff} of 500 kOe was attributed to the ferric ions. A comparison of the line intensities of the two superimposed Zeeman patterns indicated that only half of the ferric ions in Fe_3O_4 contributed to the H_{eff} of 500 kOe. A lower value of $H_{eff} = 450$ kOe was attributed to both the ferrous ions and the remaining ferric ions. The electron-exchange mechanism was said to be responsible for the lower value of H_{eff}. More recently, Kündig et al.[64] measured the relaxation time, τ, for the "electron-hopping" by the determination of the broadening of the lines corresponding to the B sites. A value of $\tau = 1.1 \pm 0.2 \times 10^{-9}$ sec was obtained at room temperature. Measurements of the internal magnetic fields yielded 491.8 $\pm$ 0.5 kOe at the A site and -460.7 ± 0.5 kOe at the B site. The assignments were in agreement with those of other workers.[63,65-67]

The effective magnetic fields at tin nuclei in substituted iron garnets of the type $Ca_xY_{3-x}Sn_xFe_{5-x}O_{12}$ were studied by Belov et al.[68] Tin, which is normally non-magnetic, will exhibit large internal magnetic fields at the nucleus when substituted into a yttrium iron garnet. The effective magnetic field was attributed to the core polarization of the electron core of the tin ions by the exchange field of the 3d electrons of the

FIGURE 6

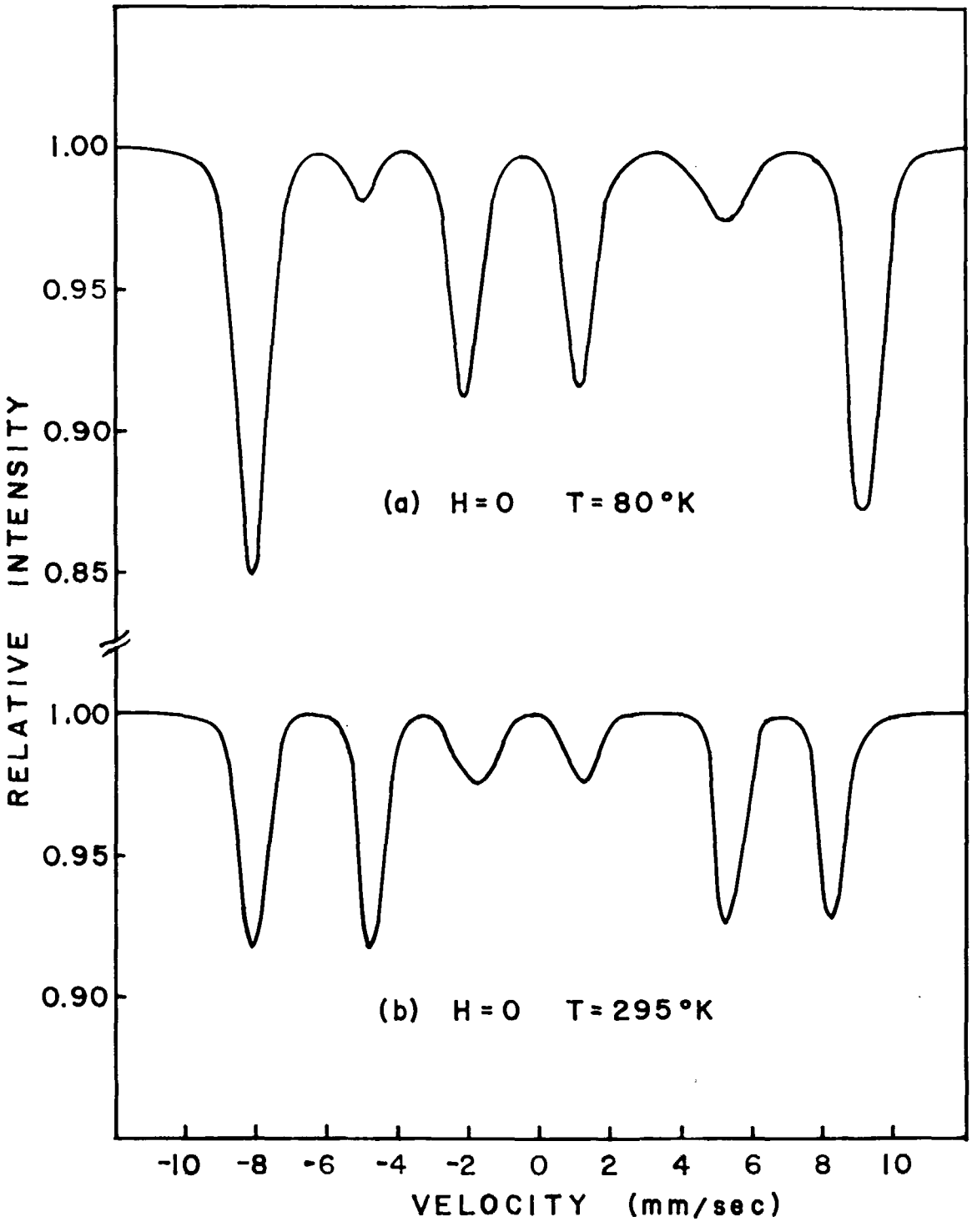

Mössbauer spectra of hematite below and above the Morin transition temperature. Blum, N., Freeman, A.J. and Shaner, J.W., *J. Appl. Phys.*, 36, No. 3 (Part 2), March 1965. With permission.

iron ions. Mössbauer spectra were recorded for samples with values of x from 0.1 to 1.5 at 77° and 295°K. Ratios of H_{eff} (77°K)/H_{eff} (295°K) were measured and the values ranged from 1.32 for x = 0.1 to 3.86 for x = 0.9. For x = 1.5, the hyperfine pattern collapsed into a single line.

In order to observe magnetic hyperfine structure in paramagnetic compounds, the electronic relaxation time must be long compared with the Larmor precession time of the nucleus. For high-spin Fe^{3+} (ground state S configuration), the spin-lattice relaxation time is usually long (10^{-6} sec) even at room temperature. The precession time of the nucleus in the hyperfine field is typically on the order of 10^{-8} sec. If the Fe^{3+} is magnetically dilute enough, a magnetic hyperfine interaction will be observed. The hyperfine spectrum of Fe^{3+} in a lattice of Al_2O_3 has been studied by Johnson et al.[69] Measurements were made on a polycrystalline sample of alumina containing 0.14% Fe_2O_3 enriched to 80% in Fe-57. The samples were prepared by compressing a mixture of Fe_2O_3 and Al_2O_3 and sintering them at 2000°C. If the 3d energy levels of Fe^{3+} are perturbed by the trigonal field of Al_2O_3, the result is a splitting of the electronic ground state into three doublets characterized by $S_z = \pm 5/2$, $\pm 3/2$, and $\pm 1/2$ where S is the electronic spin and z is the direction of the trigonal axis. Considering the various ways the nuclear spins of $I = \pm 3/2$ and $\pm 1/2$ can be coupled with the electronic spins of $\pm 5/2$, $\pm 3/2$ and $\pm 1/2$, a quite complicated Mössbauer pattern results. The observed Mössbauer spectra consisted of a superposition of three Zeeman patterns arising from the $\pm 5/2$, $\pm 3/2$ and $\pm 1/2$ electronic states. Measurements of the electronic relaxation times from the line broadening gave values of 1.4×10^{-8} sec for the spin-lattice relaxation time and 7×10^{-8} sec for the spin-spin relaxation time. A main problem in such determinations depends on finding the "true broadening" independent of other causes, such as sample thickness broadening.

Edwards et al.[70] have suggested that the isomer shift and magnetic hyperfine field parameters are more important than the quadrupole splitting in studies of chemical bonding. For high-spin Fe(III) the dominant contribution to the magnetic field at the nucleus is the core polarization field, H_s, which is negative in sign. Therefore, it is possible, according to these authors, to detect small changes in the nature of the iron-ligand bond by noting the measurably large effects produced on the effective magnetic field at the nucleus. Tetrahedral Fe(III) compounds of the type $RFeX_4^-$ where $X = Cl^-$, Br^-, or NCO^- were studied. The hyperfine field $|H_n|$ was found to be independent of the cation R^+ for $RFeCl_4^-$ and was about 470 kG. For the other ligands $|H_n|$ decreased with increasing covalency of the Fe-X bond.

Evidence for electron transfer between iron and boron atoms in iron borides with the formula Fe_2B and FeB has been obtained from the study of Mössbauer spectra.[71] In Fe_2B each boron atom has eight iron nearest neighbors at 2.18Å and two boron neighbors at 2.12Å. The boron atoms form widely spaced strings through the metal lattice, the strings being separated by about 3.6Å. Each iron atom has eleven metal neighbors at 2.41Å and four boron neighbors. The metal atoms in FeB form a distorted hexagonal lattice through which are laced zig-zag chains of boron atoms.[72,73] Each boron atom has six iron nearest neighbors at 2.15Å and two boron neighbors at 180Å, the B-B-B angle being 110°. The iron atoms have ten iron neighbors (six at 2.6-2.7Å and four at about 2.9Å) and six boron neighbors at 2.15Å.

Pauling[74,75] suggested that bonding in these borides involves electron transfer from metal to boron. Kiessling[76,77] argues that the direction of electron transfer is from boron to metal. The most direct evidence concerning the direction of electron transfer is from saturation magnetization experiments[78] and suggests a transfer in agreement with Kiessling. The results have been interpreted according to the three-band model proposed by Lundquist et al.[79,80] The three bands correspond to the 3d band of the transition metal, a 4s conduction band, and a band formed by the hybridized 2s and 2p orbitals of the boron atom.

The Mössbauer spectra of Fe_2B and FeB indicate that the considerable decrease in the internal magnetic field in passing from Fe to Fe_2B and FeB results from a reduction in the number of unpaired 3d-electrons. If one of the spin subbands is full, the decrease in internal magnetic field is said to be caused by an increase in the

number of 3d-electrons. This implies an electron transfer from boron to iron and is in agreement with the saturation magnetization result. Consistent with the magnetic field interpretation is the observed isomer shift. Small positive isomer shifts were observed for Fe_2B relative to iron and for FeB relative to Fe_2B and were attributed to an increase in population of the 3d-band.

Magnetic hyperfine studies are by no means limited to compounds of iron- or tin-substituted compounds. A considerable number of such applications have been reported for the rare earths.[81,82] It appears that with the present capability of producing magnetic fields of 60 to 80 kG in the laboratory more applications to the study of chemical bonding should be anticipated.

Metallurgy

The metallurgist is often confronted with the task of identifying various alloy phases and gaining information about precipitation phenomena and internal oxidation processes. Knowledge of the structures, compositions, and phase transformations of alloys plays a key role in determining the usefulness and service behavior of metallurgical products.

The Mössbauer technique has certainly been vital in the metallurgical applications area, especially with regard to phase identification and to the study of precipitation from solid solutions. In the iron-carbon system different phases such as martensite, austenite, ε-carbide and others can be differentiated quite unambiguously by Mössbauer spectrometry. In addition, information on the atomic scale concerning the arrangement of iron atoms and interstitial carbon atoms can be obtained. In many such ferromagnetic alloys, the value of the internal magnetic field at the iron nucleus is affected by neighboring atoms. Therefore, many of the applications which have appeared to date have been concerned with the characterization of the *local* environment of the iron atom via the magnetic hyperfine field parameter.

Austenite is a solid solution of carbon in iron where the carbon atoms occupy interstitial positions in a face-centered cubic lattice. At room temperature the Mössbauer spectrum consists of a well-defined paramagnetic singlet in the middle of a quadrupole split doublet. The central peak is indicative of iron atoms in a cubic symmetry, whereas the two satellite peaks arise from an electric field gradient at the iron nucleus and are a result of a carbon atom nearest neighbor.

Martensite is formed by the transformation of austenite at temperatures below 450°F. The transformation is relatively fast, especially when the sample is quenched. Martensite has a body-centered tetragonal structure and is ferromagnetic in contrast to austenite which is paramagnetic. The Mössbauer spectrum of martensite consists of the characteristic six-line Zeeman pattern. Because of changes in iron environments in martensitic phases, the Mössbauer spectra can be quite complex and can exhibit two or more superimposed Zeeman patterns.

Both martensite and retained austenite phases have been analyzed from their Mössbauer spectra by Moriya et al.[83] The spectra were resolved into four components as shown in Figure 7. Assuming that the carbon atoms were randomly distributed, the martensite phase was analyzed by considering the carbon atoms which have first, second, third, etc., nearest neighbor iron atoms (i.e., 1nn, 2nn, 3nn, etc.). At the top of the figure is a line diagram which illustrates the breakdown of the Zeeman components into the corresponding nearest neighbor configurations. The presence of carbon atoms produces measurable changes in the internal magnetic field, isomer shift, and quadrupole splitting from the values for pure alpha-iron, notably for the first nn Fe. This suggests that the iron-carbon bond has covalent character. The spectral parameters for the second, third and fourth nn iron atoms deviated slightly from those of α-Fe, but the signs were opposite those for the first nn iron. In Figure 8 there are plotted the internal fields of the various nn iron sites as a function of the iron-carbon distance. The first and second nearest neighbors show a marked difference in the internal field which is somewhat unexpected since the iron-carbon distance is nearly the same.

The determination of the spectral parameters is essentially routine for pure austenitic specimens. However, Christ and Giles[84] indicated that for multiphase steels (such as heat-treated carbon steels, which may contain undissolved carbides, untempered martensite, or tempered martensite as well as austenite), the accuracy of the austenite line parameters may be affected. If significant amounts of other phases (cemen-

FIGURE 7

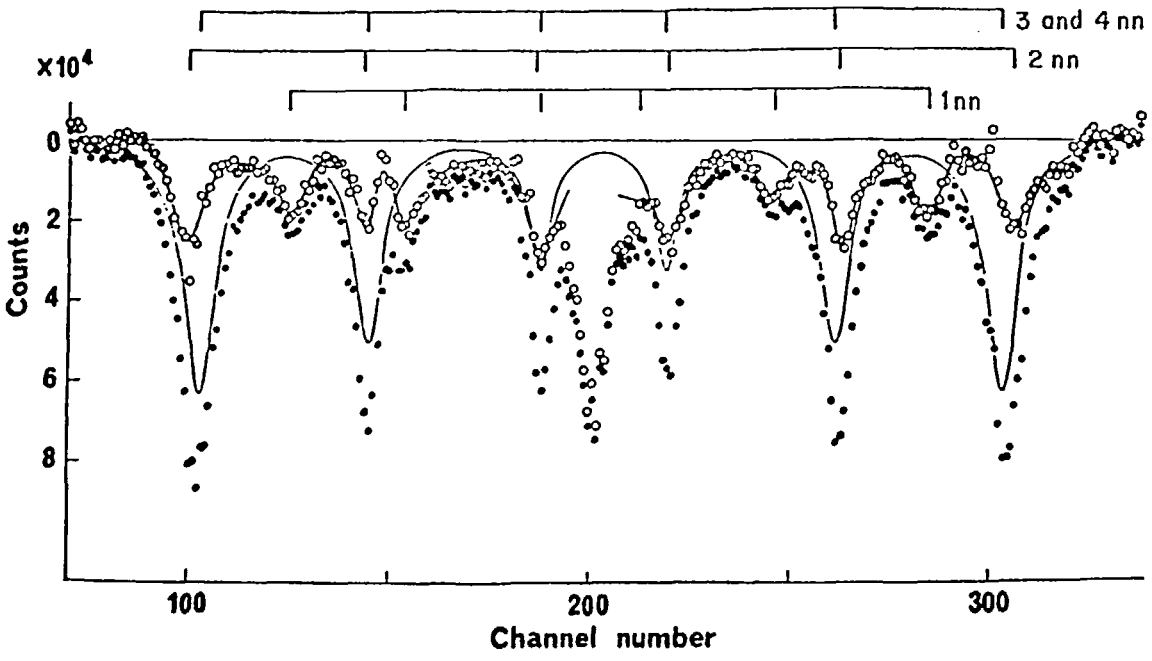

The Mössbauer spectra for the 1st, 2nd, 3rd, and 4th nearest neighbor iron atoms, respectively, assuming the iron atoms are affected by carbon atoms. Moriya, T., Ino, H., Fujita, F.E. and Maeda, Y., *J. Phys. Soc. Jap.*, 24, No. 1, 64, Jan. 1968. With permission.

tite in particular) are present, then the accuracy is diminished because of poor spectral resolution. It was suggested that the present experimental method is not suitable for the quantitative determination of austenite in bulk samples of quenched and tempered high-carbon steels.

Changes in the iron-carbon martensitic steels during the process of tempering have been studied by Ino et al.[85,86] The martensite structure of high carbon steels decomposes into the cementite (Fe_3C) and an alpha-solid solution through a series of transient metastable carbides. Since 1951 there has been some question as to whether a χ-carbide (Fe_5C_2) or a form of cementite was produced at a particular stage (stage IIIa) in the tempering of high carbon martensite.[87,88] Mössbauer spectra were recorded for a specimen which contained 5.1 atomic per cent carbon and was tempered for one hour at 140, 220, and 340°C. The spectra were then compared with the spectrum of a neat χ-carbide which was synthesized chemically.[89] The neat χ-carbide spectrum was resolved into three six-line Zeeman patterns, having internal field values of about 222, 184, and 110 kOe for the three different iron sites. The average internal field value found for the tempered specimen after step IIIa was about 194 kOe. The average positions of peaks two and five were in good agreement with those from the neat χ-carbide, but it was pointed out that the assignment of peaks one, four, and six could not be made because they were masked by the absorption of the iron matrix. These data strongly suggested that the phase produced after the tempering stage IIIa was χ-carbide.

During the room temperature aging of iron-carbon martensite the clustering of carbon atoms was observed.[90] The effect of aging was followed by observing the Mössbauer spectra as a function of time and temperature. Comparison of spectra from freshly quenched and aged samples at 20°C showed a pronounced difference in those peaks which correspond to magnetic environments. No obvious change was noted in the non-magnetic central peak. This suggested that the aging reactions at room temperature affected the martensite but not the austenite phases. Examination of the martensite Mössbauer pattern revealed three major peaks which suggested three different environments for iron. The spectra indicated that the population of two different environments for the iron atoms increased with increasing aging time while the

FIGURE 8

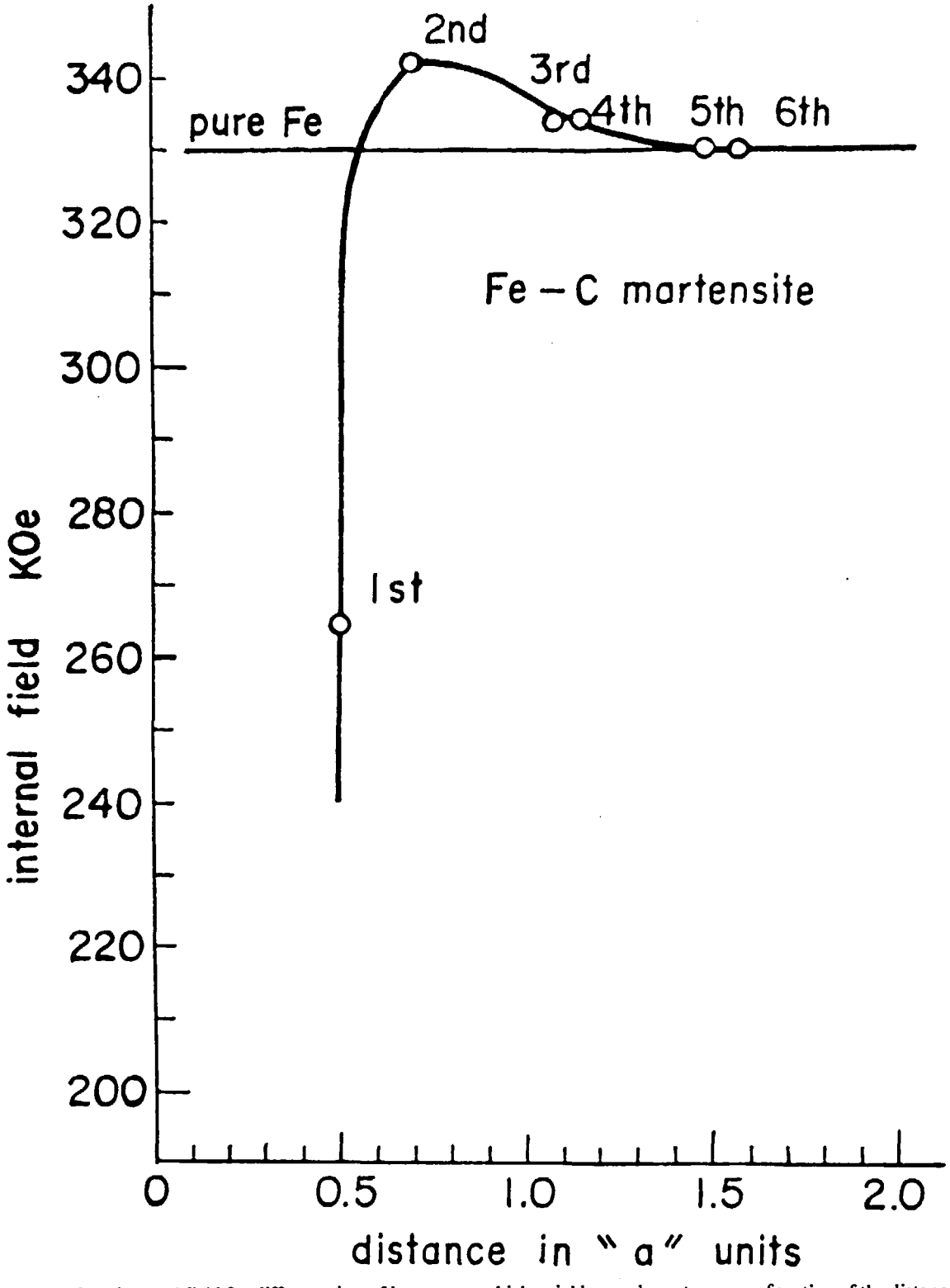

Plot of the internal field for different sites of iron atoms which neighbor carbon atoms, as a function of the distance, a, from the carbon atoms. Moriya, T., Ino, H., Fujita, F.E. and Maeda, Y., *J. Phys. Soc. Jap.*, 24, No. 1, 64, Jan. 1968. With permission.

population of the third environment decreased with time. The larger peak arose from iron atoms having no carbon neighbors while the growth of the remaining peak was attributed to the clustering of carbon atoms creating a new environment about the iron atom. A reduction in the internal field was observed for iron atoms having one isolated carbon neighbor or a cluster of carbon atoms. Also, a change in isomer shift was observed which was relatively greater for iron atoms with an isolated carbon atom environment than for iron atoms which were near a cluster. It was noted that the carbon atom indirectly influences the isomer shift by displacing the iron atom and forcing it closer to its neighbors. The kinetics of the carbon clustering were studied at 0, 10, and 20°C. The first stage corresponded to the initial formation of the cluster in the martensite matrix while the formation of ε-carbide occurred in the second stage. An empirical activation energy was calculated which was in good agreement with that found for the diffusion of carbon in ferrite.

From experimental studies of the aging effect on Fe-Cr alloys, proposals for explaining the aging mechanism were made. Some theories maintained that the aging process involved the precipitation of some minor phases such as carbides, oxides, or nitrides; the formation of superlattices; the precipitation of Cr-rich clusters, and others.[91] Yamamoto[91] has used the Mössbauer technique to study the aging of Fe-Cr alloys at 500°C. The chromium content was varied from 20 to 46.5% by weight. Samples were prepared, heated for one hour at 1100°C, and then quenched in water. The aged specimens were prepared by further annealing at 500°C for 150 hours. Comparison of quenched with aged specimens clearly showed a large increase (an average of 30%) in the value of the internal magnetic field at the iron nucleus for the aged samples. The samples with greater chromium concentration exhibited a larger increase in the internal field. This was interpreted as resulting from clusters of about 12 weight per cent chromium which have precipitated along with chromium-rich clusters in a paramagnetic state. From the line broadening that was observed in the spectra for aged specimens, it was suggested that the precipitated iron-rich phases were present in a disordered state. The isomer shift, although not accurately determined for the quenched samples, did exhibit a positive increase with increasing chromium content. This implied that the s-electron density at the iron nucleus was decreasing and probably caused by a lattice expansion upon the addition of chromium, or by an electron-transfer mechanism directed from iron to chromium atoms.

Until now, most of the Mössbauer experiments have employed transmission geometry which usually requires extensive sample preparation. With continued progress in the development of the back-scattering mode of operation, the samples used will need little or no preparation. The technique would then be more flexible, and will be perhaps more attractive to physical and applied metallurgists as both a research tool and as a routine adjunct technique. It is hoped that further Mössbauer research in metallurgy will attempt a systematic correlation of physical properties such as tensile strength, hardness, stress, corrosion, etc., with the Mössbauer spectral parameters.

Solid-State

The solid state can be represented by a quantitized system characterized by acoustic (phonon) and vibrational (optical) energy states. Some simple and useful models have been used to characterize the phonon spectrum in lattice dynamics, principally the Einstein and Debye models. The Einstein model is the simplest and treats the emitting or absorbing atoms as harmonic oscillators, each vibrating with a characteristic single frequency. The Debye treatment is a further extension of this harmonic approximation but treats the atoms as consisting of a number of oscillators with characteristic frequencies which are multiples of some frequencies, ω to ω_{max}. An expression can be written which relates ω_{max} to the Debye temperature, Θ_D, for the solid and is

$$h\omega_{max} = \kappa\Theta_D \qquad (7)$$

In the Debye harmonic approximation, the Debye-Waller factor f, often referred to as the probability of the Mössbauer effect (or recoil-free fraction), can be written as

$$f = \exp(-\langle x^2\rangle/\chi^2) \qquad (8)$$

where $\chi = \lambda/2\pi$, with λ the gamma radiation wavelength, and where $\langle x^2 \rangle$ is the mean-square displacement of the emitting or absorbing atom from its equilibrium position.

The interpretation of the f-factor using the Debye approximation is useful but, at the same time, falls short of an accurate description of the lattice dynamical picture. It is only valid for a monoatomic lattice of identical atoms. In reality, where emitting or absorbing nuclei are present as minor constituents in a host matrix, or where in addition to the phonon modes the optical modes are excited, the Debye model does not provide an accurate description. The form of the frequency distribution must be known in such cases in order to derive the relevant relationships for the f-factor. In addition, for crystal symmetries less than cubic, the Debye model is not appropriate.

Measurements of f can provide information about $\langle x^2 \rangle$ and relative Mössbauer atom-nearest-neighbor interactions. Experimentally, both relative and absolute measurement of the f-factor can be made. The relative measurements depend on comparing different "thin" absorbers against the same emission lines. The "black absorber" technique has been used to obtain absolute f values. A more complete description of the experimental techniques employed can be found in reference 92. Because of the inherent difficulties in making absolute measurements, uncertainties in f no better than $\pm 15\%$ are usually quoted. Housley[93] has described the principal, and not so obvious, errors encountered in making relative and absolute f measurements. Uncertainties in the background and peak area measurements are the major contributors to the estimated uncertainty in f. It was stated that accuracies on the order of $\pm 1\%$ could be obtained if enough attention was paid to background corrections, and considering certain other sources of error which are often ignored. Among these latter are (a) resonant nuclear self-absorption in the source, (b) inelastic electronic scattering in the source, (c) non-resonant nuclear absorption in the absorber, (d) inelastic electronic scattering, and (e) resonant nuclear scattering (re-emission) in the absorber. Accurate values of f would have important implications for making absolute quantitative analytical measurements (see section on Analytical Chemistry). The self-inversion of resonant gamma peaks has been demonstrated by Mössbauer et al.[94] They suggest that absolute f measurements could be made using this technique. To date, however, no applications have been reported.

The physicochemical significance of the Debye-Waller factor could be demonstrated by considering the work of Bukshpan et al.[95] and of Hazony[96] on the lattice-dynamical interpretation of the molecular crystal SnI_4. Measurements were made on Sn^{119} and I^{129}, both Mössbauer nuclei, over the temperature range $85° < T < 220°K$. The temperature dependence of the Debye-Waller factor was used to study the normal mode vibrations in SnI_4, which is tetrahedral. Nine (3N-6) normal vibrational modes are expected, four of which have been observed for aqueous SnI_4 by infrared or Raman spectroscopy.[97-99] The frequencies are $\upsilon_1 = 149cm^{-1}(\Theta_1 = 215°K)$, $\upsilon_2 = 47cm^{-1}(68°K)$, $\upsilon_3 = 216cm^{-1}(311°K)$, and $\upsilon_4 = 63cm^{-1}$ (91°K). Because the Debye model is not appropriate for the molecular solid, Hazony rewrote equation 8 in the form

$$f = \exp\left(-K^2 \Sigma_i \langle x_i^2 \rangle\right) \qquad (9)$$

where the summation is overall the inter- and intramolecular vibrations in which the Mössbauer atoms participate. The purpose of his treatment was to obtain characteristic Einstein temperatures for intermolecular translational and rotational vibrations. The tin atom was described as being in the molecular center of mass where its motion could be described by two characteristic frequencies, represented by two effective temperatures. A lower effective Θ_1 characterized the intermolecular translational lattice vibrations, and a higher effective $\Theta_h = 311°K$ characterized the intramolecular vibrations of the tin atom. From the l/nf–T data[95] Θ_1 was 44°K and very close to the value reported for a weak IR absorption band (48°K).[99] This indicated that most of the thermal energy of the intermolecular translational vibrations was in the optical band. From equation 9 four intramolecular frequencies are expected for the iodine atoms which describe the nine normal intramolecular vibrations: the intermolecular translational vibrations, Θ_1, already known from the tin experiment, and Θ_{rot}, the rotational vibra-

tions. A value of Θ_{rot} of 66°K was found, but no other experimental information was available by which it could be correlated. It was suggested that comparison with low-temperature thermodynamic measurements could perhaps provide a crosscheck on the value of Θ_{rot}.

Stöckler et al.[101] have shown that the Debye-Waller factor is much larger at room temperature for compounds of tin with intermolecular chemical bonds than for similar non-polymeric molecules. A compound with a coordination number of six often possesses an increased f-factor and a decreased temperature dependence. In a study of linear and crosslinked ferrocene polymers,[102] the sharp increase of the f-factor accompanied by a corresponding decrease in its temperature dependence was demonstrated. For polymeric compounds of the type $(\phi_2SnO)_n$, Goldanskii[103] found that a change in the halide substituent in the *para*-position of the phenyl ring had little effect on either the isomer shift or quadrupole splitting. A marked influence was observed in the absorption intensity suggesting an increase in the f-factor.

In a study of the charge states and environments of Fe^{57} ions embedded in single crystals of sodium chloride, some interesting observations were made.[104] The problem was to identify from the Mössbauer spectra the isolated iron ions substitutionally replacing the Na^+ ions in the sodium chloride lattice, and the iron ions which were associated with the charge-compensating positive-ion vacancies. The absorption intensity for each of the two cases was studied as a function of temperature. At high temperature (300 to 500°K) the absorption intensity, which was proportional to the f-factor for the iron atoms associated with the vacancies, was approximately four times as great as the intensity for the isolated substitutional iron atoms. This result was qualitatively explained on the basis of the difference in charge states of the iron atoms in the two environments which resulted in a difference in force constants. The iron ions associated with the vacancies were identified as Fe^{2+} and Fe^{3+} which strongly attract the neighboring chloride ions. This leads to an increase in the binding of the iron atom and effectively reduces its mean-square displacement. Therefore, in this case, the f-factor would be expected to increase as was observed. It was also suggested that differences in the symmetries and in the net mass of the two defect structures should be considered.

In the discussion of the Debye-Waller factor up to this point, only isotropic vibrations of the Mössbauer atom in the crystal were considered. However, in the case of vibrational anisotropy, the Debye-Waller factor becomes anisotropic also. This was shown originally by Karyagin.[105] Measurements of the f-factor along the three principal crystallographic axes in single crystals will yield information about the mean-square displacements (i.e., $\langle x^2 \rangle$, $\langle y^2 \rangle$, and $\langle z^2 \rangle$) in the respective directions. Some precise measurements of the anisotropy in single crystals of sodium nitroprusside have recently been made.[106] Values for the mean-square displacement tensor of the iron sites and the orientation parameters relative to the crystal axes were obtained. But from the reported data, it was not clear how the f-factor was related to the chemical bonding in this compound.

The Debye-Waller factor could, in principle, furnish information about the chemical bonding in compounds. The number of studies by the Mössbauer method have thus far been severely limited by the experimental difficulties in obtaining accurate values over a wide temperature range. The use of helium refrigerators coupled with precise temperature regulation of the sample should facilitate these measurements over an adequate temperature range.

Mineralogy

In order to obtain structural information about mineral phases, the geologist often requires accurate knowledge of atomic distributions and site occupancies. With this information some conclusions can be drawn about the past history of mineral samples. Because the formal oxidation state, coordination number, and electronic configuration at different crystallographic sites in minerals can, in principle, be obtained by Mössbauer spectrometry, the geologist is now equipped with a powerfully unique and sensitive research tool. In addition, the Mössbauer technique can be used for the detection of cation order-disorder and site occupancy factors. Many of the applications to date are concerned with iron distribution, especially in complex silicate structures. Information about the distribution of

iron over non-equivalent crystallographic sites in minerals can provide data for estimating thermodynamic quantities such as distribution isotherms and the free energy of order-disorder. Through the determination of the local magnetic field at the iron sites, differences in chemical bonding at the non-equivalent sites can be obtained. The determination of the atomic distribution and site occupancy factors can also be made by X-ray diffraction techniques but these methods are usually more laborious. The accuracy of X-ray diffraction may also be more limited for these applications.

Evans et al.[107] and Ghose and Hafner[108] have studied minerals of the orthopyroxene series. The orthopyroxenes are important rock-forming minerals with compositions similar to the $MgSiO_3$–$FeSiO_3$ system. Their structures consist of single silicate chains (SiO_3) held together by Mg^{2+} and Fe^{2+} in octahedral coordination. There are two non-equivalent octahedral positions, M_1 and M_2, which can be occupied by Mg^{2+} and Fe^{2+} in all proportions. The Mössbauer spectrum consists of two overlapping quadrupole split patterns that were assigned to two non-equivalent Fe^{2+} sites in the crystal structure. The occupancies of the Fe^{2+} sites were approximately determined, and confirmed the high-degree of Mg–Fe ordering in these minerals found previously by X-ray diffraction. Heat treatment of a sample at 1000°C caused considerable disorder in the crystal structure. The quadrupole splitting values were in agreement with those previously reported.[109,110] The possibility that the two line patterns could be composed of the overlapping of several patterns, indicating that the iron occupied more than one set of sites, was not ruled out. Based on the known crystal structure of the orthopyroxenes, Fe^{2+} was believed to be distributed mainly over two non-equivalent sites. In Table 2 there are presented the approximate Fe–Mg distribution and site-occupancy factors in a series of orthopyroxenes.[107] It was pointed out that if the Debye-Waller factors were different at the two sites or if the spectra showed a Karyagin effect, a systematic error would result. Fe^{2+} site occupancy factors could be more precisely determined from Mössbauer spectra taken at liquid nitrogen temperatures because the resolution of the Fe^{2+} doublets at M_1 and M_2 is improved considerably.[111,112]

Iron in four different crystallographic sites has been identified in the cummingtonites $(Mg,Fe)_7Si_8O_{22}(OH)_2$.[113] An inner doublet was assigned to Fe^{2+} at the M_4 site while Fe^{2+} at the M_1, M_2, and M_3 sites was represented by an outer doublet. The site occupancy factors of the four cation sites were estimated by Mössbauer and IR spectroscopy and the site population estimates were made with a stated accuracy of ±5%.

Studies of the thermal decomposition of amosite and crocidolite have been reported by Whitfield and Freeman[114] and are represented by the equations:

$$\underset{\text{crocidolite}}{Na_2Fe_2^{3+}Fe_{2.6}^{2+}Mg_{0.4}Si_8O_{22}(OH)_2} \xrightarrow{600°C} Na_2Fe_2^{3+}Fe_{2.6}^{2+}Mg_{0.4}Si_8O_{23} + H_2O$$

$$\xrightarrow{600°C} \underset{\text{acmite}}{NaFe^{3+}Si_2O_6} + \underset{\text{spinel}}{(Fe^{2+}, Mg)Fe_2^{3+}O_4} + \underset{\text{cristobalite}}{SiO_2}$$

On the basis of the isomer shift and quadrupole splitting values, the Fe^{2+} and Fe^{3+} ions were assigned to the appropriate sites in the crystal structure.

The application of a magnetic field can, in some cases, provide valuable information. In fayalite (Fe_2SiO_4) iron is present in two crystallographic sites. Below the Néel point, the two sites possess distinct local magnetic fields. Kündig et al.[115] found that the effective magnetic field, H_{eff} at one site, is parallel to one of the principal axes of the EFG tensor while the H_{eff} of the other site is not. This permitted the assignment of the smaller value of H_{eff} to the M_2 site. No conclusion could be made concerning the orientation of H_{eff} at the M_1 site with respect to the crystallographic axes. In a study of orthoferrosilite,[116,117] a large difference in H_{eff} at M_1 and M_2 was observed and was said to be unusual for sites with the same coordination

number. The smaller magnetic field at M_2 suggested that Fe^{2+} at this site was more covalently bonded than Fe^{2+} at M_1, and was consistent with the observed trend in isomer shift and interatomic distances.

In the perovskite series, $La_{1-x}Sr_xFeO_y$, Shimony and Knudsen[118] suggested the existence of an intermediate $Fe^{3+} \leftrightarrow Fe^{4+}$ state. A single narrow line was observed in the spectra with an isomer shift somewhere between the Fe^{3+} and Fe^{4+} regions. The electrical conductivity measurements of Waugh[119] were in agreement with these results. A correlation between the total isomer shift and the Fe^{4+} content was also attempted.

Tin Mössbauer spectra have been obtained for eleven tin-containing minerals at ambient and liquid nitrogen temperatures.[120] Both Sn(II) and Sn(IV) could be identified in these minerals from their isomer shift values.

Herzenberg[121] has collected Mössbauer spectra of a number of igneous rocks and marine sediments in order to demonstrate the use of the Mössbauer technique for (a) the qualitative identification of rock types, (b) the detection and identification of magnetic phases, and (c) total iron and ferric to ferrous ratio determinations. To identify rock types on the basis of Mössbauer line position patterns alone can be misleading; hence, caution should be exercised. It is not sufficient to characterize spectra derived from certain rock types only by the isomer shift and quadrupole splitting values. Such spectra may not be unique for the identification of that particular rock type. For example, Bancroft et al.[122] have noted that the quadrupole splitting decreases with increasing iron content for olivine at the M_1 and M_2 sites, for orthopyroxene at the M_2 site, and for cummingtonite at the M_4 site. Hence, the ΔE_q values are certainly not unique for these minerals and are dependent on the iron composition. All three Mössbauer parameters of isomer shift, quadrupole splitting, and magnetic hyperfine splitting should be measured and their temperature dependence determined if possible. This would result in a more accurate identification. In any case, data from other techniques should also be obtained to assist in making positive identifications.

Chemical Applications

Numerous publications have appeared which deal with chemical applications of Mössbauer

TABLE 2

Approximate Fe-Mg Distribution and Site Occupancy Factors at M_1 and M_2*

	Fe/(Fe + Mg)	Intensity		Fraction of Fe^{2+} in $M1$		Fraction of Fe^{2+} in $M2$		Site Occupancy Factor** of Fe^{2+}	
		$A1+A2$	$B1+B2$	$A2/(A1+A2)$	$B2/(B1+B2)$	$A1/(A1+A2)$	$B1/(B1+B2)$	At $M1$	At $M2$
V2(Sweden).....	0.758	0.146	0.139	0.34	0.40	0.66	0.60	0.56	0.96
				0.37		0.63			
37218(Greenland)...	0.532	0.109	0.097	0.12	0.18	0.88	0.82	0.16	0.91
				0.15		0.85			
37218(1,000°C).....	0.532	0.140	0.130	0.23	0.32	0.77	0.68	0.29	0.78
				0.27		0.73			
37218(1,100°C).....	0.532	0.127	0.111	0.27	0.31	0.73	0.69	0.31	0.76
				0.29		0.71			
4645(Madras).....	0.280	0.142	0.118	~0		~1			

*From B.J. Evans, S. Ghose, and S. Hafner, *J. Geol.*, 75, 319, (1967).
**The sum of the site-occupancy factors of all atoms at a distinct site is equal to 1.

spectrometry. Because extensive coverage of this area is beyond the scope of this review, it is hoped that the limited number of papers which follow are illustrative of the kind of information that has been obtained by this technique.

Goldanskii et al.[123] have demonstrated that dipolar aprotic solvents such as DMF, DMSO, HMTP* interact strongly with the cationic portion of organotin molecules. This strong solvation reaction produces a marked change in the quadrupole splitting of dibutyltin dichloride in frozen solutions. The quadrupole splitting was measured for various molar ratios of solvent to dibutyltin dichloride. The ΔE_q values increased rapidly until a molar ratio of about three was reached. The degree to which each of the solvents tested affected the magnitude of the quadrupole splitting was attributed to the solvation power of the solvent.

In a study of nuclear radiation damage of polymers,[124] organotin compounds have been shown to act as protective stabilizers. The Mössbauer method was used to investigate the chemical changes in dibutyltin maleate, a stabilizer in irradiated polyethylene. The protective action of the stabilizer was studied during irradiation with Co^{60} in the range of 25-600Mrad. At a dosage rate of 100Mrad the protective effect of the stabilizer ceased.

Murin et al.[125] used $Co^{57}Cl_2$ as a dopant in silver chloride single crystals. The spectra taken at various temperatures were ascribed to a covalent Fe^{2+} ion located in a lattice site. The presence of a quadrupole doublet was attributed to the formation of a quasi-chemical complex of the Fe^{2+} ion with silver vacancies. For concentrations greater than 10^{-2} mole per cent, the spectra revealed the presence of a precipitated $Co^{57}Cl_2$ phase, while for concentrations less than 10^{-3} mole per cent, the Fe^{2+} ions were located in lattice sites in the silver chloride crystal.

The kinetics of slow reactions on the order of hours or days can be studied by means of the Mössbauer method. Spectra of a portland and an aluminous cement were taken as a function of time during hydration of the samples.[126] Figure 9 uniquely demonstrates the changes taking place in the iron constituent of the portland cement during the hydration reaction.

A study of ammonia adsorption on a supported iron catalyst[127] suggested that the iron atoms were present on the surface in both the divalent and trivalent state. A catalyst was prepared by impregnating silica gel with Fe^{57} enriched ferric nitrate. After calcining in air at 500°C, the catalyst was reduced by alternately adding hydrogen and outgassing at 450°C. This preparation is shown in spectrum A of Figure 10. Spectrum B was obtained by exposing the preparation to ammonia. Partial recovery of the original preparation by outgassing is shown in Spectrum C. Peaks 1 and 3 of an overlapping quadrupole doublet were assigned to iron in one site where the spectral parameters were characteristic of high-spin Fe^{2+}. Peak 2 of Spectrum A was presumably produced by high-spin Fe^{3+}, if the assumption was made that ammine radicals were formed by the chemisorption of ammonia on the catalyst. The reaction of the ammine radicals with Fe^{3+} on the surface is shown in Spectrum B. The reversibility of the surface compound was demonstrated by outgassing the sample and obtaining Spectrum C. The conclusions made were that the probable state of the iron on the catalyst was a mixed ferrous-ferric oxide in the form of small particles on the surface of the silica gel. In addition, the ferric ions were said to occupy positions very near the surface because they reacted readily to the chemisorption of ammonia.

Analytical Chemistry

The magnitude of resonant absorption is related to the concentration of absorbing nuclei through the expression[128]

$$\varepsilon = \frac{I_\infty - I_o}{I_\infty} = f_S \left[1 - e^{-T_A/2} J_o (iT_A/2) \right] \quad (10)$$

where ε is the Mössbauer fraction of resonant radiation absorbed, and I_∞ and I_o refer to the transmitted intensities for nonresonant and resonant absorption, respectively. The concentration of absorbing nuclei, m, is usually incorporated in the "effective absorber thickness" term, T_A, which is equal to $f_A\sigma_o$, $\alpha_A m t_A$. The terms f_S and f_A are the Debye-Waller factors for the source and absorber, respectively; σ_o is the cross section for nuclear resonance; α_A is

*DMF: dimethylformamide
DMSO: dimethylsulfoxide
HMTP: heptamethyltriamidophosphate

FIGURE 9

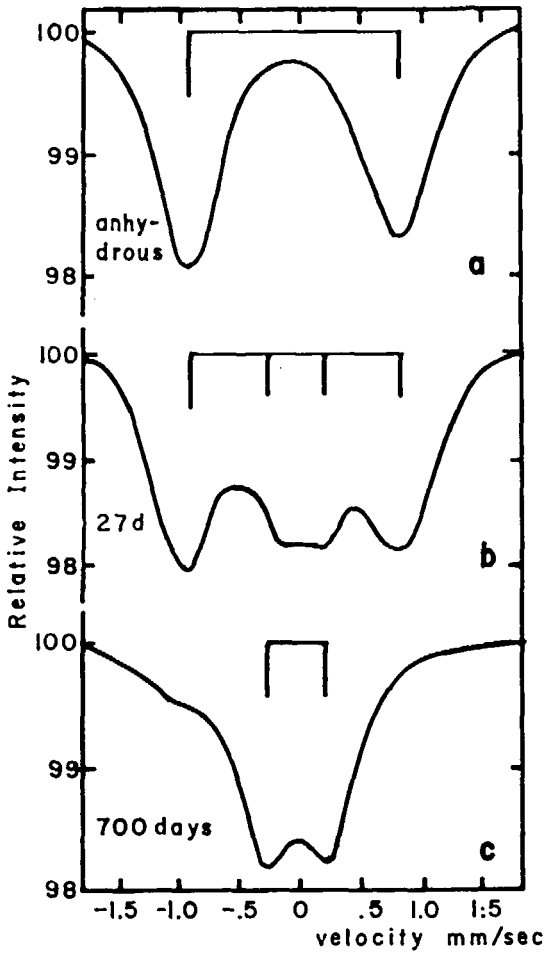

Absorption spectra of the ferrites in portland cement (PZ 375 H, W/C = 1.0) measured at various times after gaging. Wittmann, Folker, Pobell, Frank, and Wiedemann, Werner, *Z. Angewandte Phys.*, 19, No. 44, p. 20. With permission.

the isotopic abundance of the Mössbauer nuclide, and t_A is the sample thickness. J_0 is the zero-order Bessel function with an imaginary argument. Because f_A depends on the lattice dynamic characteristics of the Mössbauer atoms in the sample, an absolute determination of the number of Mössbauer atoms requires accurate knowledge of f_s and f_A. In addition, the transmission of nonresonant radiation, I_∞, through the sample is accompanied by background radiation (I′) from the source and possibly some fluorescent X-rays from the sample. This unwanted radiation will appear in the window of the single channel analyzer. The baseline of the Mössbauer spectrum then comprises the contributions from I_∞ plus I′ as shown in Figure 11. Therefore, the quantities f_S, f_A, and I′ must be accurately measured for an absolute chemical analysis to be feasible by this method. As yet, however, there has appeared no systematic evaluation of these quantities for quantitative chemical applications. Most likely this situation obtains because of the experimental difficulty in determining the Debye-Waller factors from temperature measurements which are, at present, very tedious. It appears that such an application must await advances in the pertinent experimental technology, particularly in the adaption of cryogenic equipment to Mössbauer spectrometers, to facilitate these measurements. In a manner analogous to analytical spectrophotometry, quantitative analysis for a specific element could be performed by dissolving the sample and incorporating the analate in a reproducible matrix. A series of standards in an identical matrix would then serve as the basis for a calibration curve. Pella et al.[129] reported on some of the problems

FIGURE 10

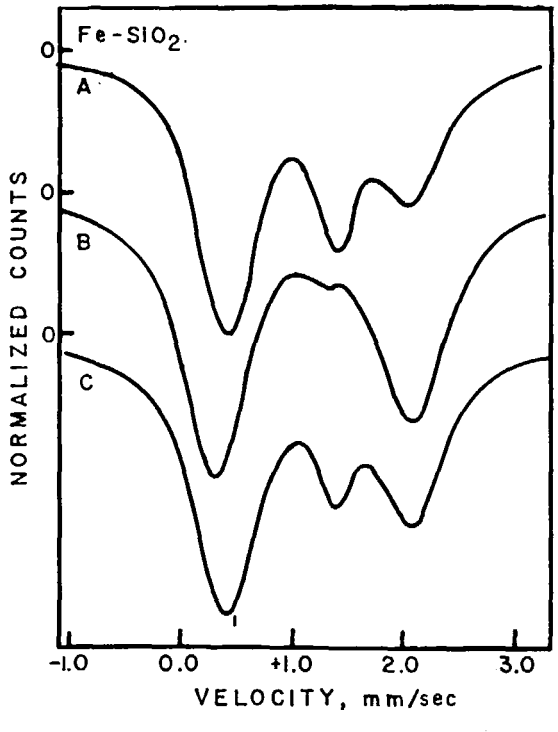

Spectra of ammonia chemisorption on a highly dispersed Fe SiO_2 sample. (a) Initial sample reduced in H_2. (b) After adding NH_3 to 1.35 torr, and (c) After outgassing at 100°C. Hobson, M.C.Jr., *Electrochemical Society Reviews and News*, July 1968. With permission.

FIGURE 11

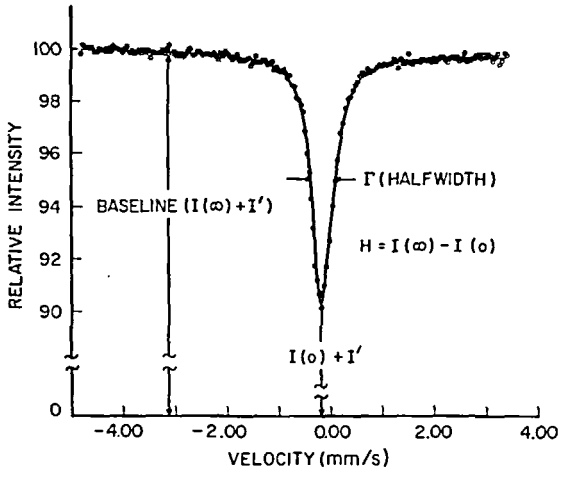

Mössbauer spectrum of SnO_2 in Al_2O_3

encountered in using this approach for the analysis of tin in tin-bearing materials. The effect of variables such as drift in detector response, sample thickness, and sample concentration was investigated, using Pd_3Sn^{119m} as a source and synthetic samples of SnO_2 in an Al_2O_3 matrix as absorbers. The data were well approximated by a Beer's law relationship at low concentration of absorbing nuclei, and the relationship can be written

$$H/B = f' [1 - e^{-K'm/2}] \qquad (11)$$

where $H/B = (I_\infty - I_o)/(I_\infty + I')$; f' and K' are empirical constants where f' is a function of f_S, and K' includes the terms f_A, σ_o, α_A and t_A. The results indicated that I' was virtually constant over a forty-fold concentration range. Of the variables studied, the source-sample-detector geometry is the most critical and must be held constant. In addition, such factors as selective absorption filters, a high resolution detector, and production of a source with a minimum of high-energy contaminants were considered in an effort to optimize the absorption signal by reducing I'. In principle, a reduction in I' could also be realized by utilizing the internal standard technique. The ratio of the absorption area (or height) of the analate (or reference standard) to that of the internal standard should be independent of the baseline of the Mössbauer spectrum and hence I'. Therefore, an analytical curve can be obtained which is practically independent of the differences in I' between samples of varying matrix composition, or between samples and reference standards.

The Mössbauer technique has met with some limited success in the non-destructive determination of the oxidation state of iron in a variety of materials. For this determination to be valid, the Debye-Waller factors for the ferrous and ferric species in the material must be identical. Yoshioka et al.[130] determined the Fe(II)/Fe(III) ratios in synthetic iron phosphate glasses which were prepared under carefully controlled conditions.[131] The spectrum consisted of two quadrupole doublets where one line of each doublet overlapped. Two methods for making background corrections were introduced for the 14.4 keV gamma peak, but the reason for these corrections was not clear; particularly since the quantity of interest is the ratio, rather than the absolute values, of the absorption areas. Ratios of Fe^{3+}/Fe^{2+} from 1.6 to 4.5 were measured with a standard deviation of a single measurement of $\pm 10\%$. The results obtained were comparable with those from chemical analysis. Small differences in the isomer shift and quadrupole splitting between various Fe^{3+} phases, as well as between Fe^{2+} phases in some oxide and phosphate mixtures, were observed.[132] It was suggested that some basic structural information on the phases should be made available before the Mössbauer analysis was carried out. Natural and synthetic samples of vivianite, $Fe_3(PO_4)_2 \cdot 8H_2O$, were measured, using calibration curves prepared from mixing ferrous and ferric phosphates in known proportions. For Fe^{3+}/Fe^{2+} ratios in the range from 0.6 to 1.0, agreement between the Mössbauer results and chemical analysis was within $\pm 3\%$. But for ratios about 4 a discrepancy of the order of 19% was observed. For accurate estimation of Fe^{3+}/Fe^{2+} ratios in mixtures of minerals it was suggested that calibration curves for each particular mixture may be required. Herzenberg[121] has measured Fe^{3+}/Fe^{2+} ratios in a variety of minerals and reported relatively poor agreement between the Mössbauer and the chemical analytical results. The greatest discrepancies between methods were found in cases where the Fe^{3+}/Fe^{2+} ratios were especially high or low. Large deviations were also observed in the study of alkali-iron silicate glasses.[133]

Joye and Axtmann[134] used a procedure for the quantitative analysis of corrosion products formed on the surface of an iron foil. A corrosion film was formed by exposing a pure iron foil to an atmosphere of HCl, H_2O and air. The weight per cent of uncorroded metal was determined by comparing the Mössbauer absorption from pure iron and from the corrosion product after calibration by a gravimetric procedure. A parameter G was obtained which was related to the fraction of uncorroded iron. Agreement of the G values obtained by gravimetry and by the Mössbauer technique was within 3%. However, the error in the estimate of the amount of corrosion product formed (i.e., 1-G) was about 27%. The Mössbauer technique was certainly not used to advantage in this study, especially with reference to the identification of the corrosion product. The corrosion product was tentatively identified as $Fe_2O_3 \cdot 2H_2O$ but no reference spectra of hydrated Fe_2O_3 were taken in order to substantiate the conclusions.

Rossiter et al.[135] have collected Mössbauer spectra for the α, β, γ, and δ forms of FeOOH at room temperature and at 77°K. The isomer shifts for all forms have been shown to fall within the range characteristic of Fe^{3+}. The quadrupole splitting was marked in the cases of β- and γ-FeOOH, but, more significantly, β-FeOOH at 77°K splits into a six-line magnetic hyperfine pattern with an internal magnetic field of 475 ± 5 kOe. γ-FeOOH at 77°K shows only the quadrupole split doublet. The spectral parameters for the various forms of FeOOH are presented in Table 3. These results illustrate the power of the Mössbauer method when the magnetic field measurement is added as an additional parameter for qualitative identification of iron oxides. The backscatter Mössbauer technique has been used more recently[135] for the identification of surface compounds on a steel surface. A form of rust on a heavily rusted 1/8 inch steel plate was identified as β-FeOOH. This result was confirmed by an X-ray powder pattern analysis. The amplitude of the backscatter emission signal was computed in order to obtain the penetration depth. The results of this calculation are shown in Figure 12. This technique appears to be a promising one for the identification of corrosion products on iron-bearing surfaces.

APPLICATIONS TO BIOLOGY

The presence of iron in biologically important compounds has prompted the use of the Möss-

TABLE 3

Mössbauer Parameters of Iron Oxides and Iron Oxy-Hydroxides at 300°K*

Compound	Chem. Shift[a] (mm/sec)	Quad. Split (mm/sec)	Int. Magn. Field (kOe)
FeO	1.37	0.6	0
α-Fe_2O_3	0.61	0.4C	517 ± 5
γ-Fe_2O_3			
Td site	0.53[c] ± .04	0	488 ± 5
Oh site	0.67 ± .04	0	499 ± 5
α-FeOOH	0.70[c]	0 ± 0.1	364 ± 37
β-FeOOH	0.640 ± .006	0.700 ± 0.008	0
	—	—	475 ± 5[b]
γ-FeOOH	0.648 ± 0.006	0.594 ± 0.006	0
δ-FeOOH	0.76 ± .2	0. ± 0.1	0
Td site[b]	—	—	525 ± 5
Oh site[b]	—	—	505 ± 5

[a] Chemical shift relative to sodium nitroprusside standard; [b] Values are for 77°K.
[c] Corrected, by adding 0.17 mm/sec, to sodium nitroprusside standard.
*From Terrell, J.H. and Spijkerman, J.J., *Appl. Phys. Lett.*, 13, 12, 1965.

FIGURE 12

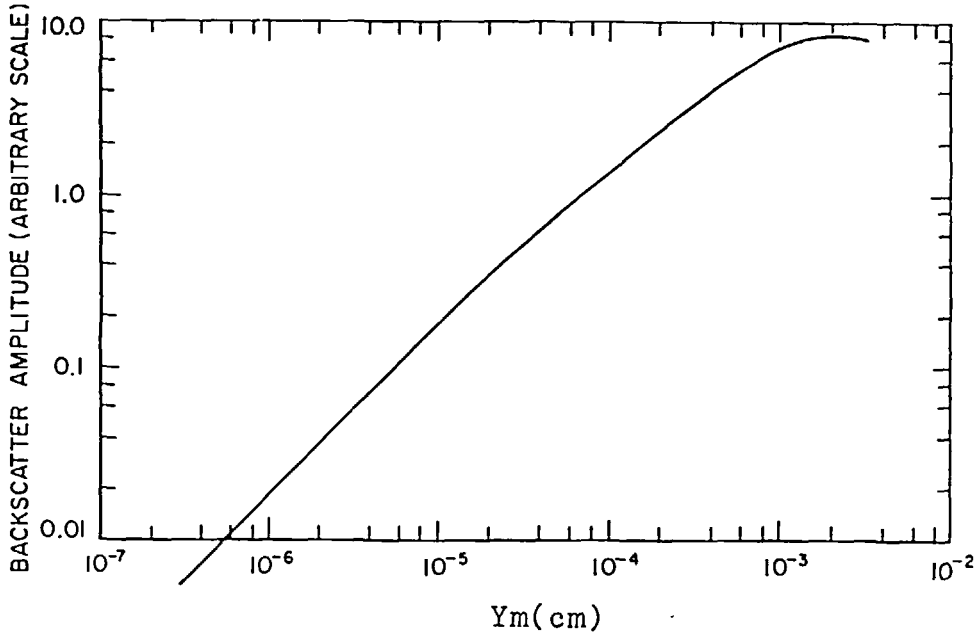

Amount of backscatter as a function of thickness of the scatterers.

bauer technique to study (a) the formal oxidation state of iron, (b) the strength of binding of iron and neighboring atoms, (c) crystal structure through the measurement of the electric field gradient, (d) electronic structure of active centers of enzymes whose prosthetic groups contain iron, and (e) the metabolism of iron in organisms using Fe^{57} as a tracer atom. One of the difficulties in the study of biological compounds is that their high molecular weights (*circa* 14,000) require enrichment of the Fe^{57} concentration in order to get adequate absorption intensity. An important step in the enrichment process is the exchange of Fe^{57} without damage to the natural structure of the compound. In order to ensure that the biological activity of the compound is not altered, the enrichment is often carried out in vivo. In the work of Gonser et al.[136] the hemoglobin of rats was enriched to 6% by maintaining the rats on a low-iron diet and then injecting them with $Fe^{57}Cl_3$ solution for one week. In many cases, an enrichment factor of 95% can be realized.

The effect of changing various ligands bound to the iron atoms in blood was studied.[136] The hemoglobin structure can be represented as:

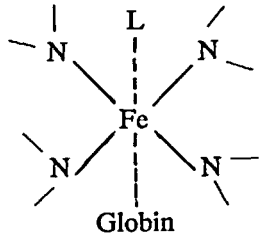

where the iron atom is located at the center of a porphyrin ring formed by four nitrogen atoms. The globin moiety is attached to iron in the 5-position, and the ligand L in the 6-position. In Figure 13 are shown the spectra obtained from the various hemoglobins. Spectra c to e were obtained by bubbling CO_2, N_2, and CO, respectively, through human blood samples at room temperature which were then frozen at 77°K. Spectra a and b are characteristic of oxyhemoglobin, whereas c, d, and e indicate the absence of oxygen in the 6-position. The similarity of spectra c and d suggests that CO_2 is not bound to iron in the 6-position, but to some other part of the molecule. The CO-hemoglobin (spectrum e) shows an absence of quadrupole splitting but has an isomer shift similar to oxyhemoglobin. The temperature dependence of the

FIGURE 13

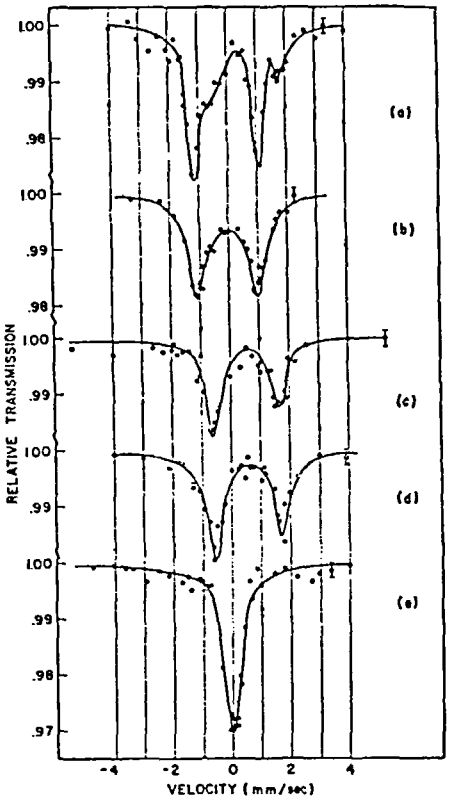

Mössbauer absorption spectra with a source of Co^{57} diffused into Pt and kept at room temperature and absorbers of (a) Rat red cells at 4° K and isotopically enriched with Fe^{57}, (b) Crystalline rat oxyhemoglobin at 77° K, (c) Human CO_2-hemoglobin (in a CO_2 atmosphere) at 77° K, (d) Human hemoglobin (in a N_2 atmosphere) at 77° K, and (e) Human CO-hemoglobin (in a CO atmosphere) at 77° K. Gonser, U., Grant, R.W., and Kregzela, J., *Science*, 143, 680, Feb. 1964. Copyright 1964 by the American Association for the Advancement of Science. With permission.

quadrupole splitting and the relative Debye-Waller factors for hemoglobin with different ligands were also reported.

A systematic study of the Fe^{2+} porphyrins (hemes) and the Fe^{3+} porphyrins (hemins) which are important constituents in hemoproteins such as hemoglobin was reported by Bearden et al.[137] These compounds containing the ethyl, vinyl, and acetyl groups as substituents in the 2- and 4-positions were examined over the temperature range 2.5 to 360°K. The interpretation of the spectra for the Fe^{2+} compounds was based on the non-equivalence between the in-plane porphyrin nitrogens and the two out-of-plane pyridine nitrogens. A tetragonal distortion from cubic symmetry would be predicted from first principles and consequently a quadrupole splitting would be expected. The Mössbauer data were in agreement with a slightly asymmetric, low-spin (S=6) electron configuration. In addition, the electron-withdrawing effect of the peripheral substituents was said to influence the non-equivalence between the in-plane porphyrin nitrogens and out-of-plane pyridine nitrogens. Therefore, a change in quadrupole splitting would be expected and related to the electron-withdrawing power of the peripheral substituents. This was demonstrated in the comparison of the values of ΔE_q for mesoheme ·(~0.6mm/sec) and diacetyldeuteroheme (~1.0mm/sec). The difference was attributed to the greater electron-withdrawing effect exerted by acetyl as compared with ethyl groups.

Among the non-heme iron proteins are the ferredoxins, an important group of proteins involved in photochemical reactions in plants and photosynthetic bacteria. The iron is believed to be close to the reactive center but the chemical form has not been unambiguously determined. Spinach ferredoxin (molecular weight 12,000) containing two iron atoms per molecule was studied by Johnson.[138] The assignment of the chemical states of the iron atoms in ferredoxin requires knowledge of all three spectral parameters. The Mössbauer spectra are shown in Figure 14 in the absence of an applied magnetic field. They consist of a superposition of two spectra, A and B. Both the oxidized and reduced forms were studied at temperatures of 195, 77, 4.2, and 1.5°K. The iron in oxidized spinach ferredoxin (spectrum A) was identified as low-spin Fe^{2+} showing no internal magnetic field at the nucleus when a magnetic field was applied. On reduction with dithionite about one-half of the iron ions are converted into high-spin Fe^{2+} (spectrum B) whereupon the application of a magnetic field splits into a magnetic hyperfine pattern. Evidence was previously found from ESR measurements that only a fraction of iron ions are affected on reduction. It was concluded that the origin of the ESR signal could not be interpreted until all the details of the Mössbauer data have been explained.

Measurements of the magnetic hyperfine field for a plant ferredoxin, an iron-sulfur protein, from green alga *Euglena* indicated that in the reduced state the effective magnetic field at the

FIGURE 14

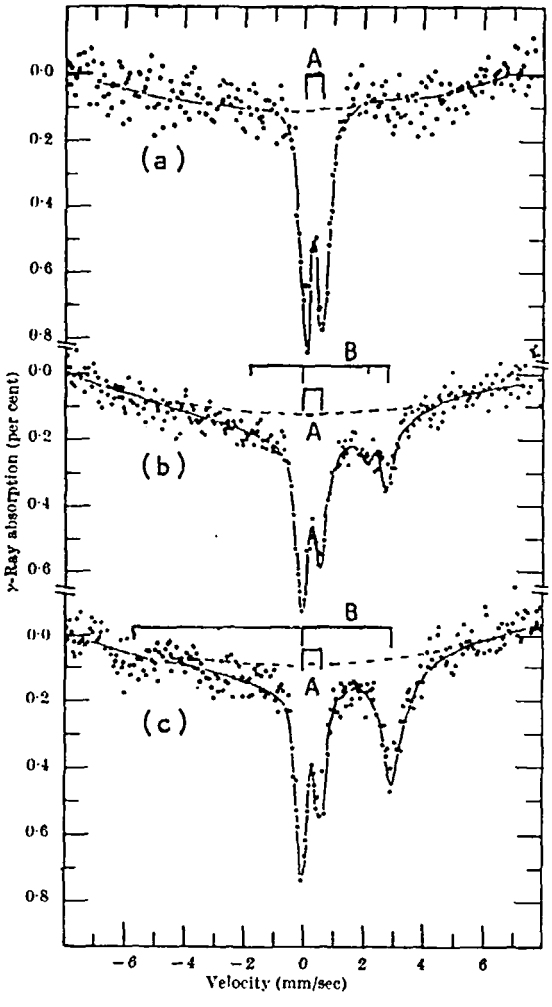

Mössbauer spectra of spinach ferredoxin. (a) Oxidized, T = 77°K (b) Reduced, T = 77°K (c) Reduced, T = 4.2°K. Johnson, C.E. and Hall, D.O., *Nature*, 217, Feb. 1968. With permission.

iron nucleus was about half that expected for typical low-spin ferric iron.[139] This suggested that a single unpaired electron was equally shared between two iron atoms.

Moss et al.[140] reported on the cc′ and c-type cytochromes from the photosynthetic bacteria Rhodospirillum rubrum and Chromatium. The two heme groups in the cytochromes were similar in iron coordination. The oxidized cytochromes cc′ have a highly distorted high-spin configuration similar to that observed for methemoglobin. However, the signs of the EFG in the respective compounds are opposite, indicating that the iron coordination is different in the two proteins. In the reduced state high-spin Fe^{2+} was identified in the cytochromes cc′ in contrast to the diamagnetic iron found in *R. rubrum* cytochrome c_2 or the *Chromatium* cytochrome c_{552}.

SUMMARY

In modern analytical chemistry it is often not sufficient to describe a material solely by indicating what kind or how much of a particular element is present in the material. There is a definite need to know in many cases something about the chemical state, structure, nature of the bonding, lattice dynamics, distribution of atomic spins, etc., for more complete physicochemical characterization. It is evident that some valuable contributions to investigations in these areas have been accomplished through the use of the Mössbauer technique. But it should be emphasized that the most objective and perhaps the most accurate interpretation of experimental data can only be accomplished when all available research tools are applied to the problem at hand. For this reason, Mössbauer spectral data should be correlated whenever possible with information from NMR, NQR, ESR, X-ray diffraction, IR and Raman spectroscopy, specific-heat, and magnetic susceptibility measurements. Some correlations of isomer shift with the spin-spin coupling constant J in nuclear magnetic resonance have already been noted for a series of organostannanes $R_{(4-n)}\ SnH_n$.[141] Independent measurements of s-electron density are potentially available from such techniques as conversion electron or photoelectron spectroscopy (ESCA). It is hoped that continued development of these methods will result in a more systematic correlation of s-electron density with the Mössbauer isomer shift.

For Fe^{57} and Sn^{119} in the presence of a quadrupolar interaction, a two-line quadrupole split pattern is observed. To obtain structural information, both the principal component V_{zz} of the EFG and the asymmetry parameter η are required and must be extracted from the spectral data. Unfortunately, for these isotopes these parameters cannot be measured directly from the spectrum, but can be obtained through the use of special experimental techniques (such as the use of single crystals or the use of an applied magnetic field). For Mössbauer nuclides, such as the rare earths, having at least one state

$I>3/2$, these parameters can be measured directly from the usual spectra. In studies of chemical structure the accuracy of conclusions made from quadrupole splitting data depend to a large extent on the correct identification of the cause of the EFG at the nucleus. This includes "valence-only" or "lattice-only" contributions or both. The use of structural models for fitting experimental quadrupole splitting data with theoretical values is especially valuable when X-ray data are not available. By altering the structural model to obtain agreement between the calculated and experimental values, the number of possibilities can be limited correspondingly.

The magnetic hyperfine splitting is somewhat unique in that the magnitude of the internal magnetic field at the nucleus is obtained directly from the Zeeman spectral pattern. It is useful to correlate this data, particularly with the NMR technique in determining Néel and Curie points, and for measurements of internal magnetic fields. Recent development of stronger Mössbauer sources together with high count-rate detection systems have greatly reduced the data acquisition time, in general, to about a few hours and, in some cases, to as little as 15 minutes. A further reduction in this time which is compatible with obtaining good precision in the spectral parameters is desirable. A spectrometer capable of fast data acquisition must be accompanied by rapid data processing so that the time elapsed between the taking of the raw data and the final computer-fitted spectrum will be as short as possible. In this regard, the use of an on-line computer interfaced with a Mössbauer spectrometer would help tremendously.

Some recent innovations in counting systems include the resonant detector which has been presently developed only for Fe^{57} and Sn^{119} applications. Such counters are characterized by a high selectivity for the Mössbauer γ-radiation with a comparatively low sensitivity for non-Mössbauer radiation. A typical Fe^{57} counter consists of a helium-methane filled proportional counter with an enriched Fe^{57} foil used as an exit window. The entering Mössbauer gamma-ray is resonantly absorbed in the enriched foil window. Upon the reemission (fluorescence) of the gamma-ray, conversion electrons of 8 keV in energy are produced and detected by the counter. Resonant detectors are still in an early stage of development and require further work to improve their efficiencies which are currently very low compared to a standard proportional counter. Further improvements in these detectors would have an important impact for metallurgical studies in conjunction with the Mössbauer backscattering mode of operation. For such applications surface layers of iron-bearing materials could be studied where the sample itself is made the exit window of the electron proportional counter. Since conversion electrons are detected in only the outermost surface layers some 10 to 3000 Å deep, this technique would be valuable for studying corrosion layers, thin films, and catalytic phenomena.

The advent of the use of Coulomb excitation to populate new Mössbauer levels[142] has made it possible to extend the number of Mössbauer nuclides available for study, particularly for the rare earths. Unfortunately, the relatively high cost of a Van de Graaff generator or other similar high-energy partiele generator, which is required for this technique, will limit the number of laboratories capable of undertaking research in this area, at least in the near future.

Further investigations should be anticipated which will more fully exploit the potential information which can be derived from the temperature dependences of the isomer shift, Debye-Waller factor, quadrupole splitting, and magnetic hyperfine interactions. Although some temperature studies of these parameters have been reported, the experimental techniques employed are often cumbersome and tedious. Improvements in the adaption of refrigerators and modern cryogenic equipment to spectrometers to facilitate the obtaining of spectral data at low temperatures will perhaps enable Mössbauer spectrometry to realize its full potential as a tool for materials characterization.

ACKNOWLEDGMENTS

The authors wish to thank John C. Travis for many enlightening discussions and Mrs. Joann Wheeler for her help in the final preparation of this manuscript.

REFERENCES

1. Lee, Y.K., Eck, J.S., Oleson, J.R., Shnidman, R., Walker, J.C., and Wiggins, J.W., Systematic Study of Nuclear Moments by Mössbauer Effects Following Coulomb Excitation, in *Hyperfine Structure and Nuclear Radiations*, Matthias, E. and Shirley, D.A., Eds., North-Holland, Amsterdam, 1968, 675.
2. Ruby, S.L. and Shenoy, G.K., [to be published].
3. Kienle, P., Nuclear Information Obtained with the Mössbauer Effect, in *Hyperfine Structure and Nuclear Radiations*, Matthias, E. and Shirley, D.A., Eds., North-Holland, Amsterdam, 1968, 28.
4. DeVoe, J.R. and Spijkerman, J.J., *Anal. Chem.*, 38, 382R, 1966.
5. DeVoe, J.R. and Spijkerman, J.J., *Anal. Chem.*, 40, 472R, 1968.
6. Muir, A.H.Jr., Ando, K.J., and Coogan, H.M., *Mössbauer Effect Data Index (1958-1965)*, Interscience Publishers, Division of John Wiley & Sons, New York, 1966.
7. *Chemical Applications of Mössbauer Spectroscopy*, Goldanskii, V.I. and Herber, R.H., Eds., Academic Press Inc., New York, 1968.
8. NBS Miscellaneous Publication, 260-13.
9. Gabriel, J.R. and Ruby, S.L., *Nucl. Instrum. Methods*, 36, 23, 1965.
10. Technical Note 404, DeVoe, J.R., Ed., National Bureau of Standards, Washington, D.C., 1966.
11. Protop, C. and Nistor, C., *Rev. Roum. Phys.*, 12, 653, 1967.
12. Ingalls, R., *Phys. Rev.*, 133, A787, 1964.
13. Webb, G.A., *Coordin. Chem. Rev.*, 4, 107, 1969.
14. Nozik, A.J. and Kaplan, M., *Phys. Rev.*, 159, 273, 1967.
15. Clark, M.G., Bancroft, G.M., and Stone, A.J., *J. Chem. Phys.*, 47, 4250, 1967.
16. Dale, B.W., Williams, R.J.P., Edwards, P.R., and Johnson, C.E., *Trans. Faraday Soc.*, 64, 3011, 1968.
17. Collins, R.L., *J. Chem. Phys.*, 42, 1072, 1965.
18. Matsen, F.A., *J. Amer. Chem. Soc.*, 81, 2023, 1959.
19. Dahl, L.F. and Ballhausen, C.F., *Mat. Fys. Medd. Dan. Vid. Selsk.*, 33, 1961.
20. Shustorovich, E.M. and Dyatkina, M.E., *Dokl. Akad. Nauk. SSSR*, 128, 1234, 1959.
21. Edwards, P.R., Johnson, C.E., and Williams, R.J.P., *J. Chem. Phys.*, 47, 2074, 1967.
22. Spijkerman, J.J., Ruegg, F.C., and May, L., The Use of Mössbauer Spectroscopy in Iron Coordination Chemistry, in *Mössbauer Effect Methodology*, Vol. 2, Gruverman, Irwin J., Ed., Plenum Press, New York, 1966, 85.
23. Walker, L.R., Wertheim, G.K., and Jaccarino, V., *Phys. Rev. Lett.*, 6, 98, 1961.
24. Danon, J., *Tech. Rept. Ser. Intern. At. Energy Agency*, 50, 89, 1966.
25. Danon, J., *J. Chem. Phys.*, 39, 236, 1963.
26. Danon, J., *J. Chem. Phys.*, 41, 3387, 1964.
27. Shulman, R.G. and Sugano, S., *J. Chem. Phys.*, 42, 39, 1965.
28. Epstein, L.M., *J. Chem. Phys.*, 40, 435, 1964.
29. Collins, R.L. and Pettit, R., *J. Chem. Phys.*, 39, 3433, 1963.
30. Gibb, T.C., Greatrex, R., Greenwood, N.N., and Thompson, D.T., *J. Chem. Soc., A.*, 1663, 1967.

31. Cordey-Hayes, M., *J. Inorg. Nucl, Chem.*, 26, 915, 1964.

32. Cordey-Hayes, M., ^{119M}Sn: Inorganic Compounds, Metals and Alloys, in *Chemical Applications of Mössbauer Spectroscopy*, Goldanskii, V.I. and Herber, R.H., Eds., Academic Press, New York, 1968, Chap. 5, 316.

33. Zuckerman, J.J., *J. Inorg. Nucl. Chem.*, 29, 2191, 1967.

34. Lees, J. and Flinn, P.A., *Phys. Lett.*, 19, 186, 1965.

35. Zuckerman, J.J., Applications of Sn^{119M}Mössbauer Spectroscopy to Chemical Problems in *Mössbauer Effect Methodology*, Vol. 3, Gruverman, Irwin J., Ed., Plenum Press, New York, 1967, 15.

36. Bearden, A.J., Marsh, H.S., and Zuckerman, J.J., *Inorg. Chem.*, 5, 1260, 1966.

37. Kamenar, B. and Grdenic, D., *J. Chem. Soc.*, 770, 1961.

38. Donaldson, J.D. and Senior, B.J., *J. Chem. Soc., A*, 1796, 1966.

39. Hoppe, R. and Dahne, W., *Naturwissenschaften*, 49, 254, 1962.

40. Bocquet, J-P., Chu, Y.Y., Kistner, O.C., Perlman, M.L., and Emery, G.T., *Phys. Rev. Lett.*, 17, 809, 1966.

41. Lees, J. and Flinn, P.A., *J. Chem. Phys.*, 48, 882, 1968.

42. Kistner, C., Jaccarino, V., and Walker, L.R., *The Mössbauer Effect*, Compton, D.M.J. and Schoen, A.H., Eds., John Wiley & Sons, Inc., New York, 1962, 264.

43. Boyle, A.J.F., Bunbury, D. St. P., and Edwards, C., *Proc. Phys. Soc. London*, 79, 416, 1962.

44. Bryukhanov, V.A., Delyagin, N.N., Opaljenko, A.A., and Shpinel, V.S., *Zh. Eksperim. i Teor. Fiz.*, 43, 432, 1962, [translation: Soviet Phys.—JETP 22, 485, 1963.]

45. Bersuker, I.B., Goldanskii, V.I., and Makaraov, E.F., *Zh. Eksperim. i Teor. Fiz.*, 49, 699, 1965. [translation: Soviet Phys.–JETP 22, 485, 1966.]

46. Greenwood, N.N. and Ruddick, J.N.R., *J. Chem. Soc.*, 1679, 1967.

47. Addison, C.C. and Simpson, W.B., *J. Chem. Soc.*, 775, 1966.

48. Ono, K. and Ito, A., *J. Phys. Soc. Jap.*, 17, 1012, 1962.

49. Gilad, P., Greenshpan, M., Hillman, P., and Shechter, H., *Phys. Lett.*, 4, 239, 1963.

50. Cinader, G., Flanders, P.J., Shtrikman, S., *Phys. Rev.*, 162, 419, 1967.

51. van der Woude, F., *Phys. Status Solidi*, 17, 417, 1966.

52. Simkin, D.J. and Bernheim, R.A., *Phys. Rev.*, 153, 621, 1967.

53. Kistner, O.C. and Sunyar, A.W., *Phys. Rev. Lett.*, 4, 412, 1960.

54. Dzyaloshinsky, I., *J. Phys. Chem. Solids*, 4, 241, 1958.

55. Moriya, T., *Phys. Rev.*, 120, 91, 1960.

56. Hrynkiewicz, A.Z. and Kulgawczuk, D.S., *Acta Phys. Polon.*, 24, 689, 1963.

57. Hrynkiewicz, A.Z., Kulgawczuk, D.S., and Tomala, K., *Phys. Lett.*, 17, 93, 1965.

58. Naish, V.E. and Turov, E.A., *Phys. Metals Metallogr.*, 11, 321, 1961.

59. Verwey, E.J.W. and de Boer, J.H., *Rec. Trav. Chim.*, 55, 531, 1936.

60. Verwey, E.J.W. and Heilmann, E.L., *J. Chem. Phys.*, 15, 174, 1947.

61. Verwey, E.J.W., Haaijman, P.W., and Romeijn, F.C., *J. Chem. Phys.*, 15, 181, 1947.

62. Verwey, E.J.W. and Haaijman, P.W., *Physica*, 8, 979, 1941.

63. Bauminger, R., Cohen, S.G., Morinov, A., Ofer, S., and Segal, E., *Phys. Rev.*, 122, 1447, 1961.

64. Kündig, W. and Hargrove, R.S., *Solid State Communications*, 7, 223, 1969.

65. Sawatzky, G.A., Coey, J.M.D.,and Morrish, A.H., *J. Appl. Phys.*, 40, 1402, 1969.

66. Ono, K. and Ito, A., *J. Phys. Soc. Jap.*, 19, 899, 1964.

67. van der Woude, F., Sawatzky, G.A., and Morrish, A.H., *Phys. Rev.*, 167, 533, 1968.

68. Belov, K.P. and Lyubutin, I.S., *Soviet Physics JETP*, 22, 518, 1966.

69. Johnson, C.E., Cranshaw, T.E., and Ridout, M.S., Proceedings of the International Conference on Magnetism, Nottingham, 1964, Institute of Physics and the Physical Society, London, 459, 1965.

70. Edwards, P.R. and Johnson, C.E., *J. Chem. Phys.*, 49, 211, 1968.

71. Cooper, J.D., Gibb, T.C., Greenwood, N.N., and Parish, R., *Trans. Faraday Soc.*, 60, 2097, 1964.

72. Kiessling, *Acta Chem. Scand.*, 4, 209, 1950.

73. Lundquist, *Arkiv Fysik*, 23, 65, 1962.

74. Pauling, *Proc. Roy. Soc., Ser. A*, 196, 343, 1949.

75. Pauling and Kiessling, *J. Electrochem. Soc.*, 98, 518, 1951.

76. Kiessling, *J. Electrochem. Soc.*, 98, 166, 1951.

77. Kiessling, *Fortschr. Chem. Forsch.*, 3, 41, 1953.

78. Weiss and Forrer, *Ann. Phys.* (Paris), 12, 279, 1929.

79. Lundquist, *Arkiv Fysik*, 23, 65, 1962.

80. Lundquist, Meyers, and Westin, *Phil. Mag.*, 7. 1187, 1962.

81. Nowik, I., Mössbauer Studies of Rare-Earth Intermetallic Compounds, in *Mössbauer Effect Methodology*, Gruverman, Irwin J., Ed., Plenum Press, New York, 1966, 147.

82. Clifford, A.F., Mössbauer Spectroscopy of the Rare Earths, in *The Mössbauer Effect and Its Application in Chemistry*, Gould, Robert F., Ed., American Chemical Society, Washington, D.C. 1967, Chap. 8, 113.

83. Moriya, T., Ino, H., Fujita, F.E., and Maeda, Y., *J. Phys. Soc. Jap.*, 24, 60, 1968.

84. Christ, B.W. and Giles, P.M., *Trans. Met. Soc. AIME*, 242, 1915, 1968.

85. Ino, H., Moriya, T., Fujita, F.E., and Maeda, Y., *J. Phys. Soc. Jap.*, 22, 346, 1967.

86. Ino, H., Moriya, T., Fujita, F.E., Maida, Y., Ono, Y., and Inokuti, Y., *J. Phys. Soc. Jap.*, 25, 88, 1968.

87. Crangle, J. and Sucksmith, W., *J. Iron Steel Inst.* (London), 168, 141, 1951.

88. Jack, K.H., *J. Iron Steel Inst.* (London), 169, 26, 1951.

89. Bernas, H., Campbell, I.A., and Fruchart, R., *J. Phys. Chem. Solids*, 28, 17, 1967.

90. Genin, Jean-Marie R. and Flinn, P.A., *Trans. Met. Soc. AIME*, 242, 1419, 1968.

91. Yamamoto, H., *J. Appl. Phys.* (Japan), 3, 745, 1964.

92. Goldanskii, V.I. and Makarov, E.F., Fundamentals of Gamma-Resonance Spectroscopy, in *Chemical Applications of Mössbauer Spectroscopy*, Goldanskii, V.I. and Herber, R.H., Eds., Academic Press, New York, 1968, Chap. 1, 24.

93. Housley, R.M., *Nucl. Instrum. Methods*, 35, 77, 1965.

94. Mössbauer, R.L., Seelbach, H.E., Persson, B., Bent, M., and Longworth, G., *Phys. Lett.*, 28A, 94, 1968.

95. Bukshpan, S. and Herber, R.H., *J. Chem. Phys.*, 46, 3375, 1967.

96. Hazony, Y., *J. Chem. Phys.*, 49, 159, 1968.

97. Stammreich, A., Forneris, R., and Tavares, Y., *J. Chem. Phys.*, 25, 1278, 1956.

98. Pistorius, C.W.F.T. and Hearhoff, P.C., *Z. Phys. Chem.* (Frankfurt), 19, 202, 1959.

99. Pistorius, C.W.F.T., *J. Chem. Phys.*, 28, 514, 1958.

100. Gerbaux, X. and Handy, A., *J. Phys. Radium*, 23, 877, 1962.

101. Stöckler, H.A., Sano, H., and Herber, R.H., *J. Chem Phys.*, 47, 1567, 1967.

102. Belov, V.F., Vishnyakova, T.P., Goldanskii, V.I., Makarov, E.F., Paushkin, Ya. M., Sokolinskaya, T.A., Stukan, R.A., and Trukhtanov, V.A., *Dokl. Akad. Nauk SSSR*, 159, 831, 1964.

103. Goldanskii, V.I., Makarov, E.F., Stukan, R.A., Trukhtanov, V.A., and Khrapov, V.V., *Dokl. Akad. Nauk SSSR*, 151, 357, 1963.

104. Mullen, J.G., *Phys. Rev.*, 131, 1415, 1963.

105. Karyagin, S.V., *Dokl. Akad. Nauk SSSR*, 148, 1102, 1963.

106. Danon, J. and Iannerella, L., *J. Chem. Phys.*, 47, 382, 1967.

107. Evans, B.J., Ghose, S., and Hafner, S., *J. Giol.*, 75, 306, 1967.

108. Ghose, S. and Hafner, S., *Z. Kristallogr.*, 125, 1, 1967.

109. Sprenkel-Segel, E.L. and Hanna, S.S., *Geochim. Cosmochim. Acta*, 28, 1913, 1964.

110. De Coster, M., Pollak, H., and Amelinckx, S., *Phys. Status Solidi*, 3, 283, 1963.

111. Hafner, S.S. and Virgo, D., *Trans. Amer. Geophys. Union*, 49, 340, 1968.

112. Virgo, D. and Hafner, S.S., *Earth Planet Sci. Lett.*, 4, 265, 1968.

113. Bancroft, G.M., *The American Mineralogist*, 52, 1009, 1967.

114. Whitfield, H.J. and Freeman, A.G., *J. Inorg. Nucl. Chem.*, 29, 903, 1967.

115. Kündig, W., Cape, J.A., Lindquist, R.H., and Constabaris, G., *J. Appl. Phys.*, 38, 947, 1967.

116. Kalvius, G.M. and Hafner, S.S., *Bull. Amer. Phys. Soc.*, 13, 29, 1968.

117. Shenoy, G.K. and Hafner, S.S., 14th Conference on Magnetism (*J. Appl. Phys.*), 1968.

118. Shimony, U. and Knudsen, J.M., *MIT Tech. Report*, 196, 1, 1965.

119. Waugh, J.S., *MIT Tech. Report*, 152, 1960.

120. Smith, D.L. and Zuckerman, J.J., *J. Inorg., Nucl. Chem.*, 29, 1203, 1967.

121. Herzenberg, C.L. and Toms, D., *J. Geophys. Res.*, 71, 2661, 1966.

122. Bancroft, G.M., Maddock, A.G., and Burns, R.G., *Geochim. Cosmochim. Acta*, 31, 2219, 1967.

123. Goldanskii, V.I., Okhlobystin, O. Yu., Rochev, V. Ya., and Khrapov, V.V., *J. Organometal. Chem.*, 4, 160, 1965.

124. Aleksandrov, A. Yu., Berlyant, S.M., Karpov, V.L., Leshchenko, S.S., Okhlobystin, O.Yu., Finkel, E.E., and Shpinel, V.S., *Vysokomol. Soyed.*, 6, 2105, 1964.

125. Murin, A.N., Lur'e, B.G., and Seregin, P.P., *Soviet Phys.–Solid State*, 9, 1110, 1967.

126. Wittmann, Von Folker, Pobell, F., and Wiedemann, W., *Z. Angew. Phys.*, 19, 281, 1965.

127. Hobson, M.C. Jr., *J. Electrochem. Soc.*, 175C, 1968.

128. Margulies, S. and Ehrman, J.R., *Nucl. Instrum. Methods,* 12, 131, 1961.

129. Pella, P.A., DeVoe, J.R., Snediker, D.K., and May, L., *Anal. Chem.*, 41, 46, 1969.

130. Yoshioka, T., Gohshi, Y., and Kohno, H., *Anal. Chem.*, 40, 603, 1968,

131. Munekata, M., *Research Report No. 638,* (Japan Electrotechnical Lab.).

132. Lerman, A., Stiller, M., and Hermon, E., *Earth and Planet. Sci. Lett.*, 3, 409, 1967.

133. Belyustin, A.A., Ostanevich, Yu. M., Pisarevskii, A.M., Tomilov, S.B., Bai-Shi, U., and Cher, L., *Fiz. Tverd. Tela,* 7, 1447, 1965.

134. Joye, D.D. and Axtmann, R.C., *Anal. Chem.*, 40, 876, 1968.

135. Terrell, J.H. and Spijkerman, J.J., *Appl. Phys. Lett.*, 13, 12, 1968.

136. Gonser, U., Grant, R.W., and Kregzde, J., *Science,* 143, 680, 1964.

137. Bearden, A.J., Moss, T.H., Caughey, W.S., and Beaudreau, C.A., *Proc. Nat. Acad. Sci. U.S.,* 53, 1246, 1965.

138. Johnson, C.E. and Hall, D.O., *Nature,* 217, 446, 1968.

139. Johnson, C.E., Elstner, E., Gibson, J.F., Benfield, B., Evans, M.C.W., and Hall, D.O., *Nature,* 220, 1291, 1968.

140. Moss, T.H., Bearden, A.J., Bartsch, R.G., and Cusanovich, M.A., *Biochemistry,* 7, 1583, 1968.

141. May, L. and Spijkerman, J.J., *J. Chem. Phys.*, 46, 3272, 1967.

142. Stevans, R.R. Jr., Eck, J.S., Ritter, E.T., Lee, Y.K., and Walker, J.C., *Phys. Rev.*, 158, 1118, 1967.